

Phonons in random alloys: The itinerant coherent-potential approximation

Subhradip Ghosh, P. L. Leath, and Morrel H. Cohen

*Department of Physics and Astronomy, Rutgers, the State University of New Jersey,
136 Frelinghuysen Road, Piscataway, New Jersey 08854-8019*

(Received 26 August 2002; published 30 December 2002)

We present the itinerant coherent-potential approximation (ICPA), an analytic, translationally invariant, and tractable form of augmented-space-based multiple-scattering theory¹⁸ in a single-site approximation for harmonic phonons in realistic random binary alloys with mass and force-constant disorder. We provide expressions for quantities needed for comparison with experimental structure factors such as partial and average spectral functions and derive the sum rules associated with them. Numerical results are presented for Ni₅₅Pd₄₅ and Ni₅₀Pt₅₀ alloys which serve as test cases, the former for weak force-constant disorder and the latter for strong. We present results on dispersion curves and disorder-induced widths. Direct comparisons with the single-site coherent potential approximation (CPA) and experiment are made which provide insight into the physics of force-constant changes in random alloys. The CPA accounts well for the weak force-constant disorder case but fails for strong force-constant disorder where the ICPA succeeds.

DOI: 10.1103/PhysRevB.66.214206

PACS number(s): 72.10.Di

I. INTRODUCTION

Many aspects of the lattice-vibrational, magnetic, and electronic excitations in disordered alloys have been intensively studied both theoretically and experimentally over the past few decades. Of them, the electronic problem has been covered in most detail in recent times with the emergence of first-principles techniques which have made it possible for the theories to attain a much higher degree of accuracy and reliability. Surprisingly, this is not true for phonons despite their being not only conceptually the simplest type of elementary excitation but also the most readily accessible to detailed experiment. From the early 1960's till the early 1980's there were many experimental investigations of phonons in random binary alloys¹⁻⁵ by neutron-scattering techniques. More recent experiments have been lacking, probably due to the absence of a reliable theory. The feature which makes the theory of phonon excitations difficult is the inseparability of diagonal and off-diagonal disorder. The reason for this is that the force-constant sum rule, i.e., the force constants between a site i and its neighbors j obey the relation $\Phi_{ii} = -\sum_{j \neq i} \Phi_{ij}$, must be rigorously satisfied even if the system is disordered. In other words, a single defect at one site in the system perturbs even the diagonal Hamiltonian on its neighbors, thereby imposing environmental disorder on the force constants. Hence, any theory must include diagonal, off-diagonal, and *environmental* disorder as well in order to produce reliable results for phonons.

From the late 1960's there were many attempts to provide an adequate theory of phonons in random alloys. The first successful, self-consistent approximation was the coherent potential approximation (CPA),⁶ a single-site, mean-field approximation generally capable of dealing only with diagonal disorder (mass disorder in the context of phonons). In the early 1970's there were several studies using the CPA (Refs. 7,8) which failed to establish it as a complete answer to the phonon problem in random alloys. The discrepancies with experiment confirmed this need for a theory which could include *force-constant changes* in addition to mass disorder. Several extensions of the CPA to include off-diagonal and

environmental disorder were proposed over the next several years⁹⁻¹⁴ but only in certain very special cases, such as the separable⁹ or the additive^{10,11} limits of off-diagonal and environmental disorder, were there successes. The more general approximations¹²⁻¹⁴ produced Green's functions which either failed to retain the necessary analytic properties, the translational invariance of the averaged system, or were not fully self-consistent. Moreover, all of these extensions failed to capture the effects of multisite or cluster scatterings which give rise to additional structures in quantities such as the spectral density functions. Later attempts which met with some success for real alloy systems included the recursion method¹⁵ which can handle large clusters and treats all kinds of disorder on an equal footing. However, the recursion method is neither self-consistent nor translationally invariant when used alone. Yussouf and Mookerjee¹⁶ were able to provide a self-consistent generalization of the CPA to include two-site scattering using a recursion method in conjunction with the augmented space formalism (ASF),¹⁷ an effective method of keeping track of the configurations.

An alternative approach was provided by Kaplan, Leath, Gray and Diehl¹⁸ (KLGD) which is also based on the ASF. This approach generalized the traveling cluster approximation of Mills and Ratanavararaksha¹⁹ for diagonal disorder to include the other kinds of disorder and multisite effects. Using the diagram symmetry rule of Mills and Ratanavararaksha and the translational symmetry of the augmented-space operators, they presented a self-consistent multiple-scattering theory which allows one to work with a small number of atoms instead of treating large clusters as is done in recursion. It provides analytic, translationally-invariant approximations at all concentrations for diagonal, off-diagonal, and environmental disorder. It can be applied even to problems of charge transfer, lattice relaxation, and short-range order in the context of electronic excitations. However, they illustrated their method only with one-dimensional models and presented it in a very general and complex mathematical language.

In this paper, we present a simple, straightforward formu-

lation of the KLGD method for single-site scattering of phonons in three-dimensional lattices and provide an application of it to phonons in random alloys. We term it the itinerant coherent-potential approximation (ICPA); it maintains translational invariance, unitarity, and analyticity of physical properties while including off-diagonal and environmental disorder. In addition to demonstrating its superiority over the single-site CPA and its previous extensions, we provide insight into the physics of force-constant disorder. Our results reveal the complex interplay of forces between various atomic species in a random environment, an important phenomenon which has never been addressed properly.

In Sec. II we describe the theory, introducing the augmented-space representation and its use in constructing the self-consistent scattering theory and the single-site itinerant coherent-potential approximation. In Sec. III we derive expressions for important physical quantities such as densities of states, spectral functions, inelastic scattering cross sections, and their sum rules in terms of the configuration-averaged Green's function of the system. In Secs. IV and V we present our results on $\text{Ni}_{55}\text{Pd}_{45}$ and $\text{Ni}_{50}\text{Pt}_{50}$ alloys as test cases and compare them with experiment. Concluding remarks are presented in Sec. VI.

II. FORMALISM

In this section, we briefly sketch the rationale behind augmented space, introduce its representations, and define the notation to be used throughout the paper. We present our discussions here only in the context of phonons. The formulation of the ICPA for other kinds of excitations is closely analogous.

A. Augmented space and its representations

The description of disordered systems conventionally proceeds as follows: the dynamical behavior of a system is described by a Hamiltonian, whereas the statistical behavior of the disorder is imposed from outside. The Hamiltonian itself does not describe the full behavior of the random system, but has to be augmented with the distribution of the set of random potentials which are associated with the various configurations of the system. The physical properties are then obtained by ensemble averages over configurations. The CPA and its extensions employ this procedure.

An alternative procedure is that instead of looking at the excitations of the system as moving in a random array of disordered potentials, the excitations are considered to be moving in periodic potentials in the presence of a 'field' which specifies the disorder. The Hamiltonian, expanded to include the disorder field, then by itself completely describes the disordered system. Since the information on random configurations is already incorporated into the Hamiltonian, the configuration averaging is not a further process as in the mean-field approaches, but simply an evaluation of matrix elements. The idea of introducing a 'disorder field' to describe the random fluctuations in the system by extending the Hilbert space to include the disorder field and by representing the Hamiltonian in this new space constitutes the core of

the augmented-space formalism. The extended Hilbert space which captures the random fluctuations is called the "augmented space."

Here, we work only with a binary alloy $A_{c_A}B_{c_B}$. We assume that each lattice site is randomly occupied by an A atom or by a B atom. We wish to calculate the configuration-averaged values of the experimentally measurable physical quantities, for which we need a configuration-averaged Green's function. In particular, we shall concentrate here on the configuration-averaged displacement-displacement (one-phonon) Green's function²⁰

$$\langle\langle G_{nm}^{\alpha\beta}(t) \rangle\rangle = \frac{1}{i\hbar} \langle\langle u_n^\alpha(t); u_m^\beta(0) \rangle\rangle, \quad (1)$$

or, after Fourier transformation to the frequency domain

$$\langle\langle \mathbf{G}(\omega^2) \rangle\rangle = \langle\langle [\mathbf{m}\omega^2 - \mathbf{\Phi}]^{-1} \rangle\rangle. \quad (2)$$

In Eqs. (1) and (2) $\langle\langle \dots \rangle\rangle$ stands for both configuration and thermodynamic averaging. In Eq. (1), m, n specify lattice sites and α, β the Cartesian directions. $u_n^\alpha(t)$ is the displacement operator of an atom at the lattice site n in the direction α at the time t . In Eq. (2) a bold symbol represents a matrix for which all indices are to be understood. The semicolon denotes Bose time ordering. \mathbf{m} is the mass operator, $\mathbf{\Phi}$ is the force-constant operator, and ω is the frequency which contains a vanishingly small negative imaginary part. The masses are random

$$m_{ij}^{\alpha\beta} = m_i \delta_{\alpha\beta} \delta_{ij}, \quad (3)$$

with m_i randomly taking on the value m^Γ if species $\Gamma = A, B$ is on site i . The force constants take on the values $(\phi_{ij}^{\alpha\beta})^{\Gamma\Delta}$ if species Γ is on site i and species Δ is on site j .

It is $\langle\langle \mathbf{G} \rangle\rangle$ which carries all the dynamical informations of interest, and the essential difficulty of the theory of phonons in random systems arises from taking the configuration average of the inverse of the matrix $\mathbf{m}\omega^2 - \mathbf{\Phi}$. The augmented-space technique^{17,21} greatly facilitates this averaging. The displacements \mathbf{u} , masses \mathbf{m} , force constants $\mathbf{\Phi}$, and Greens function \mathbf{G} are defined in the dynamical Hilbert space Ψ in which the Hamiltonian of the system operates. For a binary alloy, Ψ is augmented by the space Θ of all possible atomic configurations of the system. The resulting augmented space Ω is

$$\Omega = \Psi \otimes \Theta.$$

In Ω or Θ operators are represented by symbols with superposed carets. In the configuration representation within Θ , the state of site i is specified by the single-site state $|A_i\rangle$ if A is on i and by $|B_i\rangle$ if B is on i . With respect to these states, the occupation operators $\hat{\eta}_i'^\Gamma$, $\Gamma = A, B$,

$$\begin{aligned} \hat{\eta}_i'^A |A_i\rangle &= |A_i\rangle, \hat{\eta}_i'^A |B_i\rangle = 0, \\ \hat{\eta}_i'^B |B_i\rangle &= |B_i\rangle, \hat{\eta}_i'^B |A_i\rangle = 0 \end{aligned} \quad (4)$$

are represented by the matrices

$$\hat{\eta}_i^{\prime A} = \begin{pmatrix} 1 & 0 \\ 0 & 0 \end{pmatrix}, \quad \hat{\eta}_i^{\prime B} = \begin{pmatrix} 0 & 0 \\ 0 & 1 \end{pmatrix} = \hat{\mathbf{I}}_i - \hat{\eta}_i^{\prime A}. \quad (5)$$

The configuration of the entire system is specified by the direct product of all single-site states $\Pi_i |\Gamma_i\rangle$, $\Gamma = A, B$. The mass operator for site i is given by

$$\hat{\mathbf{m}}_i' = m^A \hat{\eta}_i^{\prime A} + m^B \hat{\eta}_i^{\prime B}. \quad (6)$$

Similarly the force-constants for sites i and j are given by

$$\hat{\Phi}_{ij}' = \phi_{ij}^{AA} \hat{\eta}_i^{\prime A} \hat{\eta}_j^{\prime A} + \phi_{ij}^{AB} \hat{\eta}_i^{\prime A} \hat{\eta}_j^{\prime B} + \phi_{ij}^{BA} \hat{\eta}_i^{\prime B} \hat{\eta}_j^{\prime A} + \phi_{ij}^{BB} \hat{\eta}_i^{\prime B} \hat{\eta}_j^{\prime B}, \quad (7)$$

with the Cartesian indices understood.

Consider now a rotated representation for site i in which the basis vectors for its configuration space are given by

$$\begin{aligned} |0_i\rangle &= \sqrt{c_A} |A_i\rangle + \sqrt{c_B} |B_i\rangle, \\ |1_i\rangle &= \sqrt{c_B} |A_i\rangle - \sqrt{c_A} |B_i\rangle. \end{aligned} \quad (8)$$

Constructing the configuration average of any operator $\hat{\mathbf{A}}$ in Θ can be carried out simply by taking the expectation value of $\hat{\mathbf{A}}$ with the state

$$|f\rangle = \prod_i |0_i\rangle. \quad (9)$$

Thus $|0_i\rangle$ is the site-average state (or the virtual-crystal state), $|1_i\rangle$ describes a fluctuation away from the average state on site i , and

$$|f_i\rangle = |1_i\rangle \prod_{j \neq i} |0_j\rangle. \quad (10)$$

is the state in which there is a fluctuation or a defect in the average state $|f\rangle$ only on site i . In this fluctuation representation the occupation operators $\hat{\eta}_i^{\prime A}$ and $\hat{\eta}_i^{\prime B}$ are transformed to

$$\begin{aligned} \hat{\eta}_i^A &= \begin{pmatrix} c_A & \sqrt{c_A c_B} \\ \sqrt{c_A c_B} & c_B \end{pmatrix}, \\ \hat{\eta}_i^B &= \begin{pmatrix} c_B & -\sqrt{c_A c_B} \\ -\sqrt{c_A c_B} & c_A \end{pmatrix}. \end{aligned} \quad (11)$$

In transforming from the configuration representation to the fluctuation representation, $\hat{\mathbf{m}}'$ goes to $\hat{\mathbf{m}}$ and $\hat{\Phi}'$ to $\hat{\Phi}$, as given by Eqs. (6) and (7), respectively, with the $\hat{\eta}'^\Gamma$ of Eq. (5) replaced by the $\hat{\eta}^\Gamma$ of Eq. (11). Thus the dynamical operators $\hat{\mathbf{m}}$ and $\hat{\Phi}$ are not diagonal with respect to the number of fluctuations or defects in the fluctuation representation and can create them, destroy them, or, in the case of ϕ_{ij} , cause them to travel or "itinerate." We refer to the movement of defects induced by the off-diagonal elements of the $\hat{\eta}_i^\Gamma$ as the itineration of fluctuations to distinguish it from the propagation of phonons. However, these operators are translationally

invariant; the randomness in configuration is thus captured by translationally invariant operators in the configuration space Θ . The $\hat{\eta}^\Gamma$ operators constitute the disorder field referred to above.

Any operator $\hat{\mathbf{A}}$ in this augmented space can be represented in block form

$$\hat{\mathbf{A}} = \begin{pmatrix} \bar{\mathbf{A}} & \mathbf{A}' \\ \mathbf{A}'^\dagger & \tilde{\mathbf{A}} \end{pmatrix}, \quad (12)$$

where the bold notation \mathbf{A} implies a matrix in the site and Cartesian indices. The four elements of the block matrix are given by

$$\begin{aligned} \bar{\mathbf{A}} &= \mathbf{P} \cdot \hat{\mathbf{A}} \cdot \mathbf{P}, \\ \mathbf{A}' &= \mathbf{P} \cdot \hat{\mathbf{A}} (1 - \mathbf{P}), \\ \mathbf{A}'^\dagger &= (1 - \mathbf{P}) \hat{\mathbf{A}} \cdot \mathbf{P}, \\ \tilde{\mathbf{A}} &= (1 - \mathbf{P}) \hat{\mathbf{A}} (1 - \mathbf{P}), \end{aligned} \quad (13)$$

where \mathbf{P} , the projection operator onto the virtual-crystal state, is given by $\mathbf{P} = |f\rangle\langle f|$. Thus, we see that $\bar{\mathbf{A}}$ is the configuration average of the quantity $\hat{\mathbf{A}}$ while $\mathbf{A}', \mathbf{A}'^\dagger$ generate the coupling between the average and the fluctuation states and $\tilde{\mathbf{A}}$ is that part of \mathbf{A} entirely within the space of fluctuation states.

In the present paper we shall make the approximation of treating explicitly only single fluctuation states $|f_i\rangle$ in the fluctuation space $\Theta - |f\rangle\langle f|$, although multiple-fluctuation states are treated implicitly via a self-consistency condition. States in Ω can then be specified by $|if\rangle$ or $|if_i\rangle$ where i is the site index of the dynamical variable in Ψ , position or momentum, with the Cartesian index understood. For the site indices of the corresponding matrix elements we shall often use the compact notation

$$\begin{aligned} \langle if | \hat{\mathbf{A}} | jf \rangle &= \bar{A}_{ij}, \\ \langle if_i | \hat{\mathbf{A}} | jf_i' \rangle &= \tilde{A}_{ij}^{(l)l'}, \\ \langle if | \hat{\mathbf{A}} | jf_i \rangle &= A_{ij}^{\prime(l)}, \\ \langle if_i | \hat{\mathbf{A}} | jf \rangle &= A_{ij}^{\prime\dagger(l)}, \end{aligned} \quad (14)$$

where l and l' denote the locations of the concentration fluctuation or defect. The parentheses around l indicate that it is neither a site nor a Cartesian direction index, but indicates instead the position of a fluctuation in the lattice.

B. Multiple-scattering picture

A phonon propagating in a random alloy undergoes irreducible multiple scattering²⁸ both repeatedly off a single fluctuation and successively off fluctuations on the different sites it encounters in the process. The CPA takes into account

Multiple Scattering Picture

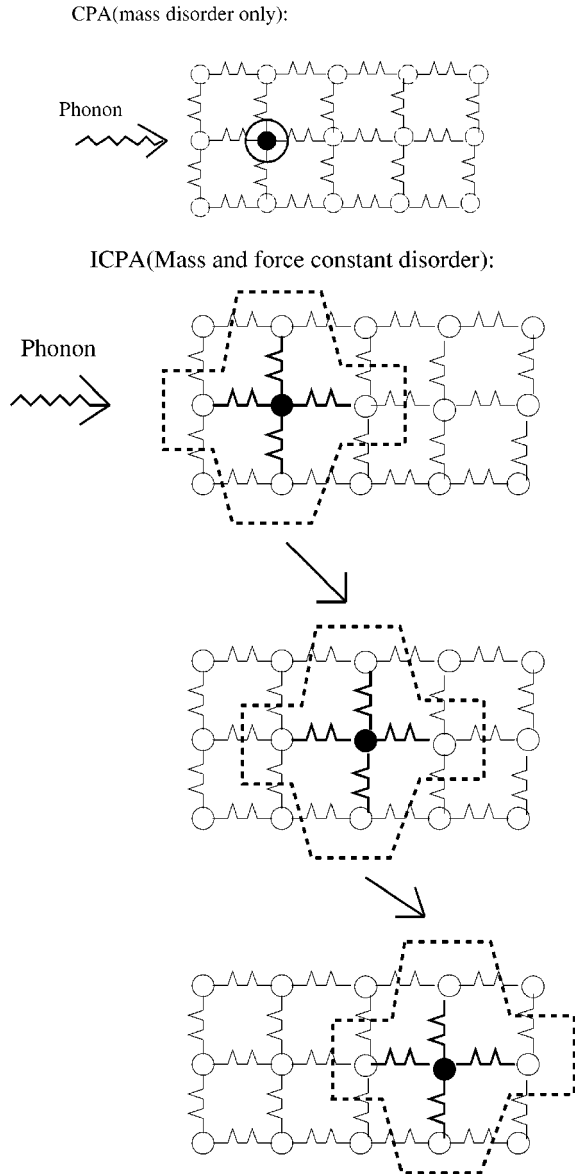


FIG. 1. Multiple scattering picture in the CPA (top) and with the ICPA (bottom). The filled circle is the site of the fluctuation and the contours around it indicate its area of influence. The arrows with the ICPA indicate the *itineration* of the fluctuation to neighboring sites. The details are given in the text.

the former but not the latter. To illustrate how the treatment of this process of multiple scattering by fluctuations differs between the CPA and our formalism we employ diagram (Fig. 1). The top panel, a two-dimensional cross section, illustrates the multiple-scattering process included in the CPA. There, the filled circle is a single “fluctuation site” immersed in an average medium denoted by open circles. The arrow on the left is the direction of phonon propagation. When the phonon meets the fluctuation site, it undergoes irreducible multiple scattering at that site. In the CPA (diagonal disorder), the irreducible scattering by the defect site is confined to the defect site. The circle around the fluctuation site indi-

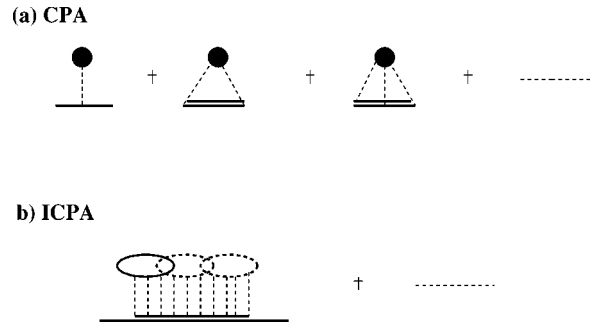


FIG. 2. The self-energy diagrams in the CPA (top) and a typical example in the ICPA (bottom). The details are given in the text.

icates the region of influence of the perturbation. None of the springs are affected by the presence of this defect since the force constants are the same everywhere. One does an averaging over all the possible occupations of the single site. The phonon diagrams of the self-energy which describe this multiple scattering process completely are shown in Fig. 2(a). There, the filled circles represent the fluctuation sites, the dotted lines represent successive scatterings from the fluctuation site, and the double solid line represents the self-consistent propagator.

The lower three panels in Fig. 1 illustrate scattering sites in the ICPA. The difference from the CPA is that the region of influence is not only the site of fluctuation but also its neighboring environment around the fluctuation site. The figure shows an example (dotted contour) where the environment includes nearest neighbors only. (The calculations could be extended to further neighbors as well.) When the phonon interacts with the fluctuation site in the top panel of the three, it scatters also from all of its neighbors since their spring constants also undergo changes (denoted by the thick spring lines in contrast to the thin ones for the average medium). The whole cluster of atoms undergoes fluctuations in force constants as the location of the fluctuation site changes. One has to keep in mind that the force constant between the fluctuation site and its neighbor on the right, say, depends on the occupation of both sites, as is true for the next neighboring site on its right as well. So, one is led to include the irreducible scatterings by the fluctuation on all neighboring sites, which then requires inclusion of scattering by the fluctuations on its neighbors, etc., until the irreducible scatterings extend throughout the entire sample. A simple example of this process is indicated in the middle and bottom panels. Indeed, Mills and Ratanavararaksha¹⁹ have shown that once there are non-diagonal terms in the scattering, the self-energy *must* include these migrations (itinerations) of the scatterer throughout the sample in order to attain unitarity and thereby guarantee that the average Green’s function will be properly analytic or Herglotz. The self-consistent scattering and the resulting coherent potential about a single defect thus itinerates from defect to defect throughout the sample, making it an itinerant coherent potential. The scattering could have started from any site in the sample so that the result is also fully translationally invariant, and the self-energy is q dependent but diagonal in the q space of the Brillouin zone of the underlying periodic lattice structure. Figure 2(b) illustrates a

typical self-energy diagram in the ICPA. The solid and dotted overlapping ellipses denote the multiple scattering by a single-site and its neighbors, i.e., by a cluster of atoms, and the subsequent iteration of this process. The thin dotted lines and the thick double lines are as in Fig. 2(a).

In the multiple scattering framework, we calculate the self-energy $\Sigma(\omega^2)$, defined by

$$\langle\langle \mathbf{G}(\omega^2) \rangle\rangle = [\mathbf{G}_{vca}^{-1}(\omega^2) - \Sigma(\omega^2)]^{-1}, \quad (15)$$

where \mathbf{G}_{vca} is the unperturbed Green's function,

$$\mathbf{G}_{vca} = (\bar{\mathbf{m}}\omega^2 - \bar{\Phi})^{-1}, \quad (16)$$

and $\bar{\mathbf{m}}$ and $\bar{\Phi}$ are the configuration-averaged mass and force-constant operators respectively.

Our major task is to calculate the self-energy $\Sigma(\omega^2)$. Let us consider $\hat{\mathbf{K}} = (\hat{\mathbf{m}}\omega^2 - \hat{\Phi}) = \hat{\mathbf{G}}^{-1}$. Using the 2×2 block representation of augmented-space operators of Eq. (12) we get

$$\hat{\mathbf{G}} = \begin{pmatrix} \bar{\mathbf{G}} & \mathbf{G}' \\ \mathbf{G}'^\dagger & \bar{\mathbf{G}} \end{pmatrix} = \begin{pmatrix} \bar{\mathbf{K}} & \mathbf{K}' \\ \mathbf{K}'^\dagger & \bar{\mathbf{K}} \end{pmatrix}^{-1}. \quad (17)$$

Using the relation for the inverse of an operator in 2×2 block form,²⁶ namely,

$$\hat{\mathbf{A}}^{-1} = \begin{pmatrix} (\bar{\mathbf{A}} - \mathbf{A}' \cdot \tilde{\mathbf{A}}^{-1} \mathbf{A}'^\dagger)^{-1} & -(\tilde{\mathbf{A}} \cdot \mathbf{A}'^{-1} \cdot \bar{\mathbf{A}} - \mathbf{A}'^\dagger)^{-1} \\ -(\bar{\mathbf{A}} \cdot \mathbf{A}'^\dagger \cdot \tilde{\mathbf{A}} - \mathbf{A}')^{-1} & (\tilde{\mathbf{A}} - \mathbf{A}'^\dagger \cdot \bar{\mathbf{A}}^{-1} \cdot \mathbf{A}')^{-1} \end{pmatrix}, \quad (18)$$

we get

$$\begin{aligned} \bar{\mathbf{G}} &= [(\bar{\mathbf{m}} \cdot \omega^2 - \bar{\Phi}) - \mathbf{K}'(\tilde{\mathbf{m}} \cdot \omega^2 - \tilde{\Phi})^{-1} \mathbf{K}'^\dagger]^{-1} = [\mathbf{G}_{vca}^{-1} - \mathbf{K}' \\ &\quad \times \{\mathbf{G}_{vca}^{-1} - [(\bar{\mathbf{m}} \cdot \omega^2 - \bar{\Phi}) - (\tilde{\mathbf{m}} \cdot \omega^2 - \tilde{\Phi})]\}^{-1} \mathbf{K}'^\dagger]^{-1} \\ &= [\mathbf{G}_{vca}^{-1} - \mathbf{K}' \cdot \mathbf{F} \cdot \mathbf{K}'^\dagger]^{-1}. \end{aligned} \quad (19)$$

Therefore, the self-energy is given by

$$\Sigma = \mathbf{K}' \cdot \mathbf{F} \cdot \mathbf{K}'^\dagger, \quad (20)$$

where

$$\mathbf{F} = \tilde{\mathbf{K}}^{-1} = \{\mathbf{G}_{vca}^{-1} \cdot \tilde{\mathbf{I}} - \tilde{\mathbf{V}}\}^{-1}, \quad (21)$$

and where

$$\tilde{\mathbf{V}} = (\bar{m} \cdot \tilde{\mathbf{I}} - \tilde{\mathbf{m}})\omega^2 - (\bar{\Phi} \tilde{\mathbf{I}} - \tilde{\Phi}). \quad (22)$$

The quantity $\tilde{\mathbf{V}}$ denotes all perturbations to the average medium and \mathbf{F} contains the iteration of the fluctuation in the average medium.

Up to this point, the scattering formalism is exact. We now introduce the ICPA by restricting the states within the configuration space $\Theta - |f\rangle\langle f|$ to the single-fluctuation states, the notation for which is given by Eq. (14). Making the site and Cartesian indices explicit, we obtain for Σ in Eq. (20), under this restriction,

$$\Sigma_{ij}^{\alpha\beta} = \sum K_{\alpha i, \delta k}^{(m)} F_{\delta k, \gamma l}^{(m)(n)} K_{\gamma l, \beta j}^{\prime \dagger (n)}. \quad (23)$$

The summations are over the repeated indices and the fluctuation iterator \mathbf{F} is given by a Dyson equation

$$\mathbf{F}^{(i)(j)} = \mathbf{G}_{vca} \left[\delta_{(i)(j)} + \sum_l \tilde{\mathbf{V}}^{(i)(l)} \cdot \mathbf{F}^{(l)(j)} \right], \quad (24)$$

where only the site index of the fluctuation is shown. The quantities in Eq. (23) are translationally invariant as follows:

$$\begin{aligned} K_{ik}^{(m)} &= K_{i-m, k-m}^{(0)}, \\ F_{kl}^{(m)(n)} &= F_{k-m, l-m}^{(0)(n-m)}. \end{aligned} \quad (25)$$

The single fluctuation in Eq. (23) can be considered to have been ‘‘created’’ by $\mathbf{K}^{\prime(n)}$ at site n , iterated to site m by $\mathbf{F}^{(n)(m)}$ and ‘‘destroyed’’ by $\mathbf{K}^{\prime \dagger(m)}$ at site m . The \mathbf{K} , $\mathbf{K}^{\prime \dagger}$, and \mathbf{F} matrices have elements which are nonzero only for site indices within the environment of the appropriate defects, i.e., the indices i and k (l and j) must be within the neighborhood perturbed by the defect at $m(n)$. The terms with more than one fluctuation (defect) present at a time correspond to coherent pair and ‘‘defect cluster’’ scattering and are neglected in the single-site scattering considered here. All of these operators act in the augmented space. The Eqs. (20)–(24) define an itinerant single-site multiple scattering theory.

C. Self-consistency

The restriction in Eq. (23) to states of $\Theta - |f\rangle\langle f|$ containing only a single fluctuation is a very severe approximation. Multiple-fluctuation states are of course present in \mathbf{F} and contribute to Σ . In the spirit of the CPA, these are included approximately by introducing self-consistency. As in the CPA (Refs. 18,20) we obtain self-consistency by replacing \mathbf{G}_{vca} in \mathbf{F} in Eq. (24) by a conditional propagator $\mathbf{G}^{(i)}$, identical to $\bar{\mathbf{G}} = \langle\langle \mathbf{G} \rangle\rangle$ except that all irreducible scatterings beginning or ending on site i are omitted, so that \mathbf{F} would then be given by

$$\mathbf{F}^{(i)(j)} = \mathbf{G}^{(i)} \left[\delta_{(i)(j)} + \sum_l \tilde{\mathbf{V}}^{(i)(l)} \cdot \mathbf{F}^{(l)(j)} \right]. \quad (26)$$

In parallel with Eq. (15), $\mathbf{G}^{(i)}$ contains a conditional self-energy $\Sigma^{(i)}$ which is similar to Eq. (23), except that it includes only those scatterings that neither start nor end on i ,

$$\mathbf{G}^{(i)} = [(\mathbf{G}_{vca})^{-1} - \Sigma^{(i)}]^{-1}, \quad (27)$$

$$\Sigma^{(i)} = \sum_{l, m \neq i} \mathbf{K}^{\prime(l)} \cdot \mathbf{F}^{(l)(m)} \cdot \mathbf{K}^{\prime \dagger(m)}. \quad (28)$$

Referring to Fig. 2(a), the double line in the multiple-scattering graphs is the propagator $\mathbf{G}^{(i)}$ when the solid dot refers to site i . We obtain the *itinerant* CPA by allowing \mathbf{K}' , \mathbf{K}'^\dagger , and $\tilde{\mathbf{V}}$ to include force-constant disorder as well and therefore defect iteration in Eqs. (26)–(28). This closed set of equations defines our single-site, self-consistent, multiple-

scattering theory which, when solved, yields \mathbf{F} . Inserting \mathbf{F} into Eq. (20) for Σ and the result into Eq. (15) then yields \mathbf{G} . It is already known that Eqs. (15),(20),(26)–(28) have a unique solution which yields a Herglotz average Green's function.¹⁸ A major difference between this and previous generalizations of the CPA is that for scattering from single-site fluctuations with off-diagonal and/or environmental disorder, as is considered here, the matrix representation of the operator $\tilde{\mathbf{V}}$ has elements which transfer or itinerate the fluctuation from site to site. This feature causes the self-energy to have nonzero off-diagonal elements in real-space extending across the sample and thus contributes importantly to such quantities as the two-particle vertex corrections in a way the CPA cannot.²⁷

It now remains to solve these equations, making use of the translational symmetry of the augmented-space operators. We accomplish this by Fourier transforms on the fluctuation-site labels

$$A(\vec{q})_{mn} = N^{-1} \sum_{l,l'} A_{l+m,l'+n}^{(l)(l')} e^{-i\vec{q}\cdot\vec{R}_{ll'}} \quad (29)$$

and

$$A_{l+m,l'+n}^{(l)(l')} = N^{-1} \sum_{\vec{q}} A(\vec{q})_{mn} e^{i\vec{q}\cdot\vec{R}_{ll'}}, \quad (30)$$

where $\vec{R}_{ll'}$ is the lattice vector connecting the fluctuation sites l and l' , m and n are neighbors of l and l' , respectively, and the \vec{q} sum is over the Brillouin zone.

We can also effect Fourier transforms on the site indices themselves. That of the self-energy is

$$\Sigma(\vec{q}) = N^{-1} \sum_{ij} \Sigma_{ij} e^{-i\vec{q}\cdot\vec{R}_{ij}}. \quad (31)$$

From Eqs. (20), (25), and (29), it follows that

$$\Sigma(\vec{q}) = \sum_{l,m,n,p} K_{lm}^{(0)} F(\vec{q})_{mn} K_{np}^{\dagger(0)} e^{-i\vec{q}\cdot\vec{R}_{lp}}. \quad (32)$$

In this notation, Eq. (26) becomes

$$F(\vec{q})_{mn} = G_{mn}^{(0)} + \sum_{rp} G_{mr}^{(0)} \tilde{\mathbf{V}}(\vec{q})_{rp} F(\vec{q})_{pn}. \quad (33)$$

The Cartesian indices here are implicit so that each quantity is a 3×3 matrix.

Since the range of interaction in real-space is finite, the perturbations $\mathbf{K}'^{(i)}$ and $\tilde{\mathbf{V}}(\vec{q})$ are finite matrices, nonzero only over a finite set of real sites. For example, if we consider nearest-neighbor perturbation only in a single-site approximation, the $\tilde{\mathbf{V}}(\vec{q})$ and \mathbf{K}' are $3(Z+1) \times 3(Z+1)$ matrices where Z is the number of nearest neighbors. This is the minimum matrix size necessary to exhibit all the impurity modes or states about each fluctuation site.

In full matrix notation, we obtain

$$\mathbf{F}(\vec{q}) = [\mathbf{G}^{(0)-1} - \tilde{\mathbf{V}}(\vec{q})]^{-1}. \quad (34)$$

These matrices, for example, for an fcc lattice, are of dimension 39×39 .

In order to evaluate $\mathbf{G}^{(0)}$ we rewrite Eq. (27) as

$$\mathbf{G}^{(0)} = [(\mathbf{G}_{vca})^{-1} - \Sigma^{(0)}]^{-1} = [\langle\langle \mathbf{G} \rangle\rangle^{-1} + \tilde{\Sigma}^{(0)}]^{-1}, \quad (35)$$

where $\tilde{\Sigma}^{(0)} = (\Sigma - \Sigma^{(0)})$. The conditional self-energy $\tilde{\Sigma}^{(0)}$ contains *only* those scatterings which either start or end with a perturbation caused by a fluctuation at site 0. Thus, to evaluate the self-consistent propagator $\mathbf{G}^{(0)}$, we need to know $\langle\langle \mathbf{G} \rangle\rangle$. But $\langle\langle \mathbf{G} \rangle\rangle$ is obtained from Eq. (15), which becomes

$$\begin{aligned} \langle\langle G(\vec{q}) \rangle\rangle &= [G_{vca}(\vec{q})^{-1} - \Sigma(\vec{q})]^{-1}, \\ \langle\langle G_{ij} \rangle\rangle &= N^{-1} \sum_{\vec{q}} \langle\langle G(\vec{q}) \rangle\rangle e^{-i\vec{q}\cdot\vec{R}_{ij}}. \end{aligned} \quad (36)$$

After reaching self-consistency by the procedure described below, we use these expressions to calculate densities of states and spectral functions.

The conditional self-energy $\tilde{\Sigma}^{(0)}$ can be broken up into two contributions: (i) Scattering that starts from a defect at site 0 and ends at site j and (ii) scattering that starts at j but ends at 0.

This decomposition results in

$$\begin{aligned} \tilde{\Sigma}^{(0)} &= \sum_j [\mathbf{K}'^{(0)} \cdot \mathbf{F}^{(0)(j)} \cdot \mathbf{K}'^{\dagger(j)} + \mathbf{K}'^{(j)} \cdot \mathbf{F}^{(j)(0)} \cdot \mathbf{K}'^{\dagger(0)}] \\ &\quad - \mathbf{K}'^{(0)} \cdot \mathbf{F}^{(0)(0)} \cdot \mathbf{K}'^{\dagger(0)}. \end{aligned} \quad (37)$$

The last term is subtracted to avoid overcounting when $j=0$.

In a block notation similar to that of Eq. (12), we have

$$\tilde{\Sigma}^{(0)} = \begin{pmatrix} \Sigma_1 & \Sigma_3 \\ \Sigma_3^\dagger & 0 \end{pmatrix}, \quad (38)$$

$$\mathbf{G}^{(0)} = \begin{pmatrix} \mathbf{G}_1^{(0)} & \mathbf{G}_3^{(0)} \\ \mathbf{G}_3^{(0)} & \mathbf{G}_2^{(0)} \end{pmatrix}, \quad (39)$$

$$\langle\langle \mathbf{G} \rangle\rangle = \begin{pmatrix} \mathbf{G}_1 & \mathbf{G}_3 \\ \mathbf{G}_3^\dagger & \mathbf{G}_2 \end{pmatrix}, \quad (40)$$

where, for a general operator $\hat{\mathbf{A}}$, \mathbf{A}_1 begins and ends with scattering about site 0, \mathbf{A}_2 neither begins nor ends with scattering about site 0 and \mathbf{A}_3 (\mathbf{A}_3^\dagger) begins (ends) with scattering at the site 0 and ends (begins) with scattering about a site different from 0. The term Σ_2 is 0 since $\tilde{\Sigma}^{(0)}$ must begin or end at the site 0. From Eq. (35), we have

$$\mathbf{G}^{(0)} = \langle\langle \mathbf{G} \rangle\rangle (\mathbf{I} + \tilde{\Sigma}^{(0)} \langle\langle \mathbf{G} \rangle\rangle)^{-1}, \quad (41)$$

which leads to

$$\mathbf{G}_1^{(0)} = \bar{\mathbf{X}} [\mathbf{I} + (\Sigma_1 - \Sigma_3 \cdot \mathbf{G}_2 \cdot \Sigma_3^\dagger) \bar{\mathbf{X}} + \Sigma_3 \cdot \mathbf{G}_3^\dagger]^{-1}, \quad (42)$$

where

$$\bar{\mathbf{X}} = (\mathbf{I} + \mathbf{G}_3 \cdot \Sigma_3^\dagger)^{-1} \mathbf{G}_1, \quad (43)$$

after a lengthy algebraic analysis which was previously given in Ref. 18.

In order to evaluate these expressions,¹⁸ we need to calculate four terms: $\mathbf{G}_1, \Sigma_1, \mathbf{G}_3 \Sigma_3^\dagger$, and $\Sigma_3 \mathbf{G}_2 \Sigma_3^\dagger$. The first term Σ_1 is just a finite sum of finite matrices and can be evaluated directly, but the other two terms involve sums which range over all sites in the solid and must be evaluated by Fourier transforms. This is done in the following way:

$$(G_3 \Sigma_3^\dagger)_{t,t'} = \sum_m \sum_{r,n,l} \langle\langle G(\omega^2) \rangle\rangle_{t,m+r} K_{m+r,m+n}^{(m)} F_{m+n,l}^{(m)(0)} K_{l,t'}^{\dagger(0)} - \sum_r \langle\langle G(\omega^2) \rangle\rangle_{t,r} \tilde{\Sigma}_{r,t'}^{(0)},$$

which becomes

$$(G_3 \Sigma_3^\dagger)_{t,t'} = \frac{1}{N} \sum_q \sum_r \langle\langle G(\vec{q}) \rangle\rangle e^{i\vec{q} \cdot \vec{R}_{tr}} M(\vec{q})_{r,t'} - (G_1 \Sigma_1)_{t,t'} \quad (44)$$

and, similarly,

$$(\Sigma_3 G_2 \Sigma_3^\dagger)_{t,t'} = \frac{1}{N} \sum_{q,r,r'} M(\vec{q})_{tr} \langle\langle G(\vec{q}) \rangle\rangle e^{i\vec{q} \cdot \vec{R}_{rr'}} M(\vec{q})_{r',t'} - (\Sigma_1 G_1 \Sigma_1 + \Sigma_1 G_3 \Sigma_3^\dagger + \Sigma_3 G_3^\dagger \Sigma_1)_{t,t'}, \quad (45)$$

where

$$M(\vec{q})_{r,t'} = \sum_{nl} K_{rn}^{(0)} F(\vec{q})_{nl} K_{lt'}^{\dagger(0)}. \quad (46)$$

In these equations, 0 is the index of the single fluctuation-site in consideration; r, r', t, t', l, n are the neighboring sites of 0; and m, m' are general sites in the sample. So, it is clear that one needs to work only on matrices of size $3(Z+1) \times 3(Z+1)$ and use the Fourier transform of operators to handle the itineration of the fluctuation throughout the entire sample. An interesting point to note is that the quantities $G_3 \Sigma_3^\dagger$ and $\Sigma_3 G_2 \Sigma_3^\dagger$ represent the scattering and itineration of the disturbance including the effect of the off-diagonal and environmental disorder. In case of diagonal-disorder only, they vanish giving $\mathbf{G}_1^{(0)} = \mathbf{G}_1 (\mathbf{I} + \Sigma_1)^{-1}$, which is the CPA self-consistent propagator, and the self-consistent set of equations reduces to the CPA equations.

The inputs to the self-consistency cycle are $\mathbf{G}_{start}^{(0)} = \mathbf{G}_{vca}$ (or some better guess), \mathbf{K}' , \mathbf{K}'^\dagger , and $\tilde{\mathbf{V}}(\vec{q})$. The procedures for evaluating the latter three quantities are given in the Appendix. The cycle consists of the following steps.

- (1) Calculation of $\mathbf{F}(\vec{q})$ using Eqs. (33) and (34).
- (2) Calculation of $\Sigma(\vec{q})$ using Eq. (32).
- (3) Calculation of $\langle\langle G(\vec{q}) \rangle\rangle$ and $\langle\langle G(\omega^2) \rangle\rangle$ using Eq. (36).
- (4) Calculation of $\mathbf{G}_1^{(0)}$ using Eqs. (42), (43), (44), and (45).

(5) If the results of steps (1)–(4) are acceptably close to those of the previous cycle, stop. If not, use as input to step 1 and iterate.

The iterations are done till self-consistency is achieved for each \vec{q} point in the Brillouin zone. In the process of achieving self-consistency, one calculates $\langle\langle G \rangle\rangle$ in both real space and in \vec{q} space; each is needed to obtain densities of states and spectral densities, respectively. In the next section, we describe how these are used to calculate physical quantities of interest and discuss their significance.

III. IMPORTANT QUANTITIES; SUM RULES

In this section we derive results for important physical quantities such as the densities of states (partial and total), spectral densities (partial and total), and inelastic scattering cross sections (coherent and incoherent) which enable us to make direct comparisons with experimental measurements.

A. Densities of states

The total density of states for a three-dimensional system is defined as

$$\nu(\omega) = \frac{1}{3\pi N} \text{Im}\{\text{Tr}\langle\langle \mathbf{m} \cdot \mathbf{G}(\omega^2) \rangle\rangle\}, \quad (47)$$

where \mathbf{m} is the mass matrix and N is the number of sites. In augmented space we have

$$\begin{aligned} \langle\langle mG \rangle\rangle_{ii} &= \langle if | \hat{\mathbf{m}} \cdot \hat{\mathbf{G}} | if \rangle, \\ &= \langle if | \hat{\mathbf{m}} | if \rangle \langle if | \hat{\mathbf{G}} | if \rangle + \langle if | \hat{\mathbf{m}} | if_i \rangle \langle if_i | \hat{\mathbf{G}} | if \rangle, \\ &= \bar{m} \bar{G}_{00} + m' \langle if_i | \hat{\mathbf{G}} | if \rangle. \end{aligned} \quad (48)$$

To evaluate the second term, we use the notation of Eq. (12) for the operators $\hat{\mathbf{G}}$ and $\hat{\mathbf{K}} = \hat{\mathbf{G}}^{-1}$. Then, using Eq. (18), we obtain

$$\langle if_i | \hat{\mathbf{G}} | if \rangle = \mathbf{G}'^\dagger = -\tilde{\mathbf{K}}^{-1} \cdot \mathbf{K}'^\dagger \cdot \bar{\mathbf{G}} = -\mathbf{F} \cdot \mathbf{K}'^\dagger \cdot \bar{\mathbf{G}}. \quad (49)$$

We can, therefore, write

$$\langle if_i | \hat{\mathbf{G}} | if \rangle = - \sum_l \sum_{j,n} F_{ij}^{(i)(l)} K_{jn}^{\dagger(0)} \langle\langle G \rangle\rangle_{ni}.$$

Fourier transforming over the fluctuation site according to Eq. (29) gives

$$\langle if_i | \hat{\mathbf{G}} | if \rangle = - \frac{1}{N} \sum_{l,j,n} \sum_q F(\vec{q})_{0j-l} e^{i\vec{q} \cdot \vec{R}_{il}} K_{j-l,n-l}^{\dagger} \langle\langle G \rangle\rangle_{ni}.$$

The Fourier transform of $\langle\langle \mathbf{G} \rangle\rangle$ on the real-site index now gives

$$\begin{aligned} \langle if_i | \hat{\mathbf{G}} | if \rangle &= - \frac{1}{N^2} \sum_{l,j,n} \sum_{\vec{q}\vec{q}'} \\ &\times F(\vec{q})_{0j-l} e^{i\vec{q} \cdot \vec{R}_{il}} K_{j-l,n-l}^{\dagger} \langle\langle G(\vec{q}') \rangle\rangle e^{i\vec{q} \cdot \vec{R}_{ni}}. \end{aligned}$$

Finally we obtain

$$\langle if_i | \hat{\mathbf{G}} | if \rangle = - \sum_{mp} \sum_q F(\vec{q})_{0,m} K_{mp}^{\prime\dagger} e^{i\vec{q}\cdot\vec{R}_p} \langle \langle G(\vec{q}) \rangle \rangle,$$

where $m = j - l$, $p = n - l$, the neighboring sites perturbed by the fluctuation. All the terms on the right hand side have been calculated already in the process of achieving self-consistency. The evaluation of the average density of states is thus straightforward.

The partial density of states for atoms of type s is given by

$$\nu(\omega)_s = \frac{m_s}{3\pi N} \text{Im} \{ \text{Tr} \langle \langle G(\omega^2)^{ss} \rangle \rangle_{ii} \}, \quad (50)$$

where

$$\langle \langle G^{ss} \rangle \rangle_{ii} = \langle \langle G^{ss} \rangle \rangle_{00} = \langle 0f | \hat{\boldsymbol{\eta}}_0^s \cdot \hat{\mathbf{G}} | 0f \rangle \quad (51)$$

because of translation invariance. We thus have

$$\begin{aligned} \langle \langle G^s \rangle \rangle_0 &= \langle \langle G^{ss} \rangle \rangle_{00} = \langle 0f | \hat{\boldsymbol{\eta}}_0^s | 0f \rangle \langle 0f | \hat{\mathbf{G}} | 0f \rangle \\ &+ \langle if | \hat{\boldsymbol{\eta}}_0^s | 0f_0 \rangle \langle 0f_0 | \hat{\mathbf{G}} | 0f \rangle, \end{aligned} \quad (52)$$

and, from Eq. (11), it follows that

$$\begin{aligned} \nu(\omega)_A &= - \frac{m_A}{3\pi} \text{Im} [c_A \{ \langle 0f | \hat{\mathbf{G}} | 0f \rangle \} + \sqrt{c_A c_B} \{ \langle 0f_0 | \hat{\mathbf{G}} | 0f \rangle \}], \\ \nu(\omega)_B &= - \frac{m_B}{3\pi} \text{Im} [c_B \{ \langle 0f | \hat{\mathbf{G}} | 0f \rangle \} - \sqrt{c_A c_B} \{ \langle 0f_0 | \hat{\mathbf{G}} | 0f \rangle \}]. \end{aligned} \quad (53)$$

The elements of $\hat{\mathbf{G}}$ in Eq. (53) were already evaluated while calculating the average density of states above.

The partial Green's functions $\langle \langle G^s \rangle \rangle_0$ are used in calculating the incoherent scattering structure factor which is directly measured in the experiments

$$\langle \langle S_{\text{incoh}}(\vec{Q}, \omega) \rangle \rangle = \sum_s b_s^2 \vec{Q} \cdot \text{Im} \langle \langle G^s(\omega) \rangle \rangle_0 \cdot \vec{Q}, \quad (54)$$

where b_s is the incoherent scattering length for atoms of type s and Q is the phonon wave number.

B. Spectral densities

The average spectral function is defined as

$$\langle \langle \mathcal{A}_\lambda(\vec{q}, \omega^2) \rangle \rangle = \frac{1}{\pi} \text{Im} \langle \langle G_\lambda(\vec{q}, \omega^2) \rangle \rangle, \quad (55)$$

where λ is a normal-mode branch index. More interesting quantities to calculate are the conditional or partial Green's functions $\langle \langle G^{ss'}(\vec{q}, \omega^2) \rangle \rangle$ in \vec{q} space because these enable one to calculate the coherent-scattering structure factors which are measured directly in the neutron-scattering experiments and are given by

$$\langle \langle S_\lambda(\vec{q}, \omega) \rangle \rangle_{\text{coh}} = \sum_{ss'} d_s d_{s'} \frac{1}{\pi} \text{Im} \langle \langle G_\lambda^{ss'}(\vec{q}, \omega^2) \rangle \rangle, \quad (56)$$

where d_s is the coherent scattering length for the species s . The conditional Green's functions are defined as

$$\begin{aligned} \langle \langle G^{ss'}(\vec{q}, \omega^2) \rangle \rangle &= \frac{1}{N} \sum_{ij} \langle \langle G^{ss'}(\omega^2) \rangle \rangle_{ij} e^{-i\vec{q}\cdot\vec{R}_{ij}}, \\ \langle \langle G^{ss'}(\omega^2) \rangle \rangle_{ij} &= \langle \langle \hat{\boldsymbol{\eta}}_i^s \hat{\mathbf{G}}(\omega^2) \hat{\boldsymbol{\eta}}_j^{s'} \rangle \rangle \\ &= \langle if | \hat{\boldsymbol{\eta}}_i^s \hat{\mathbf{G}} \hat{\boldsymbol{\eta}}_j^{s'} | jf \rangle = \langle if | \hat{\boldsymbol{\eta}}_i^s | if \rangle \langle if | \hat{\mathbf{G}} | jf \rangle \\ &\quad \times \langle jf | \hat{\boldsymbol{\eta}}_j^{s'} | jf \rangle + \langle if | \hat{\boldsymbol{\eta}}_i^s | if_i \rangle \langle if_i | \hat{\mathbf{G}} | jf \rangle \\ &\quad \times \langle jf | \hat{\boldsymbol{\eta}}_j^{s'} | jf \rangle + \langle if | \hat{\boldsymbol{\eta}}_i^s | if \rangle \langle if | \hat{\mathbf{G}} | jf_j \rangle \\ &\quad \times \langle jf_j | \hat{\boldsymbol{\eta}}_j^{s'} | jf \rangle + \langle if | \hat{\boldsymbol{\eta}}_i^s | if_i \rangle \langle if_i | \hat{\mathbf{G}} | jf_j \rangle \\ &\quad \times \langle jf_j | \hat{\boldsymbol{\eta}}_j^{s'} | jf \rangle. \end{aligned} \quad (57)$$

In Eq. (57) the index λ is to be understood. These four terms include all the possible scattering processes when two different sites are occupied by two species. The four different terms involve calculations of the Green's function under various circumstances of coupling between the average and the fluctuation states weighted by the appropriate concentrations.

We obtain from Eq. (57)

$$\begin{aligned} \langle \langle G^{ss'} \rangle \rangle_{ij} &= c_s c_{s'} \langle if | \hat{\mathbf{G}} | jf \rangle \\ &+ [c_s \sqrt{c_s(1-c_s)} (-1)^{(1-n^s)} \langle if_i | \hat{\mathbf{G}} | jf \rangle] \\ &+ [c_s \sqrt{c_{s'}(1-c_{s'})} (-1)^{(1-n^{s'})} \langle if | \hat{\mathbf{G}} | jf_j \rangle] \\ &+ c_s c_{s'} (-1)^{(n^s+n^{s'})} \langle if_i | \hat{\mathbf{G}} | jf_j \rangle. \end{aligned} \quad (58)$$

The integer n^s is equal to 1 if $s=A$ and is equal to 0 if $s=B$.

These terms can be easily calculated using Fourier transforms as has been previously demonstrated for the density of states. The final forms of the conditional Green's functions in \vec{q} space are

$$\begin{aligned} \langle \langle G^{AA}(\vec{q}, \omega^2) \rangle \rangle &= c_A^2 \langle \langle G(\vec{q}, \omega^2) \rangle \rangle \\ &\quad + c_A \sqrt{c_A c_B} (T_1 + T_2) + c_A c_B T_3, \\ \langle \langle G^{BB}(\vec{q}, \omega^2) \rangle \rangle &= c_B^2 \langle \langle G(\vec{q}, \omega^2) \rangle \rangle \\ &\quad - c_B \sqrt{c_A c_B} (T_1 + T_2) + c_A c_B T_3, \\ \langle \langle G^{AB}(\vec{q}, \omega^2) \rangle \rangle &= c_A c_B \langle \langle G(\vec{q}, \omega^2) \rangle \rangle \\ &\quad + \sqrt{c_A c_B} (c_B T_1 - c_A T_2) - c_A c_B T_3, \\ \langle \langle G^{BA}(\vec{q}, \omega^2) \rangle \rangle &= c_A c_B \langle \langle G(\vec{q}, \omega^2) \rangle \rangle \\ &\quad - \sqrt{c_A c_B} (c_A T_1 - c_B T_2) - c_A c_B T_3, \end{aligned} \quad (59)$$

where

$$\begin{aligned}
 T_1 &= \sum_{nm} F_{0n}(\vec{q}) K_{nm}'^\dagger e^{i\vec{q}\cdot\vec{R}_m} \langle\langle G(\vec{q}, \omega^2) \rangle\rangle, \\
 T_2 &= \sum_{nm} \langle\langle G(\vec{q}, \omega^2) \rangle\rangle e^{-i\vec{q}\cdot\vec{R}_n} K_{nm}' F_{m0}(\vec{q}), \\
 T_3 &= F_{00}(\vec{q}) + \sum_{nm} \sum_{lp} F_{0n}(\vec{q}) K_{nm}'^\dagger \\
 &\quad \times e^{i\vec{q}\cdot\vec{R}_m} \langle\langle G(\vec{q}, \omega^2) \rangle\rangle e^{-i\vec{q}\cdot\vec{R}_l} K_{lp}' F_{p0}(\vec{q}), \quad (60)
 \end{aligned}$$

and where n , m , l , and p are the neighboring sites of the fluctuation site 0 influenced by the perturbation. For the lattices with each site having inversion symmetry, $T_1 = T_2$ holds because T_1 and T_2 are the contributions from two processes which are conjugate to one another. In that case, $\langle\langle G^{AB}(\vec{q}, \omega^2) \rangle\rangle = \langle\langle G^{BA}(\vec{q}, \omega^2) \rangle\rangle$ when $c_A = c_B$.

The sum rules for the conditional Green's functions are derived the following way: Integrate $\omega \hat{\mathbf{G}}(\omega^2)$, Eq. (2), along the real axis, closing the contour above at infinity, obtaining

$$\oint d\omega \omega \hat{\mathbf{G}}(\omega^2) = \hat{\mathbf{m}}^{-1} \pi i$$

or

$$\int_0^\infty d\omega 2\omega \text{Im} \hat{\mathbf{G}}(\omega^2) = \hat{\mathbf{m}}^{-1} \pi. \quad (61)$$

Similarly, using Eq. (57), taking the Fourier transform of Eq. (58), carrying out the contour integral, and inserting Eq. (61) yields the sum rule for the partial spectral functions

$$\int_0^\infty d\omega 2\omega \text{Im} \langle\langle G^{ss'}(\vec{q}, \omega^2) \rangle\rangle = \pi \frac{c_s}{m_s} \delta_{ss'}. \quad (62)$$

For the total Green's function we obtain

$$\int_0^\infty d\omega 2\omega \text{Im} \langle\langle G(\vec{q}, \omega^2) \rangle\rangle = \pi \left(\frac{c_A}{m_A} + \frac{c_B}{m_B} \right). \quad (63)$$

The experimental dispersion curves are obtained from the wave-vector dependence of the peak frequencies of the structure factors as measured, after a deconvolution of the experimental resolution function. The question is whether the dispersion curves so obtained, which incorporate the effect of the coherent scattering lengths, differ significantly from those obtained from the peak frequencies of the Green's function itself which gives, in principle, a proper description of the dynamics but does not contain the scattering length weighting. To answer that question one needs to recognize that the peak positions in $\text{Im} \mathbf{G}$ are very closely related to the zeroes of $\text{Re} \mathbf{G}^{-1}$ at a given wave vector. If we diagonalize the Hermitian $\text{Re} \mathbf{G}^{-1}$ both with respect to mode and species index, each of the two species components of $\text{Re} \mathbf{G}^{-1}$ will have a zero. Correspondingly, each of the two components of $\text{Im} \mathbf{G}$ will have a peak, if $\text{Im} \Sigma$ does not wipe it out. So, in the species representation, the different matrix elements $\text{Im} G^{ss'}$ will thus all have these peaks at nearly the same

frequencies. Thus, the weighting of the $G^{ss'}$ by the scattering lengths will not shift the peak positions significantly even when the scattering lengths differ appreciably though the intensities and the line shapes of S_{coh} and $\text{Im} \mathbf{G}$ may differ significantly. In summary, the structure factor fairly accurately reflects the phonon dynamics contained in \mathbf{G} with regard to the dispersion curves, an important fact illustrated below in the next two sections where we present our calculations on $\text{Ni}_{55}\text{Pd}_{45}$ and $\text{Ni}_{50}\text{Pt}_{50}$ alloys.

IV. APPLICATION TO $\text{Ni}_{55}\text{Pd}_{45}$; WEAK FORCE-CONSTANT DISORDER

In $\text{Ni}_{55}\text{Pd}_{45}$ alloy, the mass disorder is much larger than the force-constant disorder. The mass ratio $m_{\text{Pd}}/m_{\text{Ni}}$ is 1.812, whereas the Pd force constants are only about 15% larger than those of Ni.^{22,23} In $\text{Ni}_{50}\text{Pt}_{50}$ alloy, both the mass disorder and the force-constant disorder are large, providing an interesting contrast between the two materials. For both the cases we have done our calculations on 200 ω points and have used a small imaginary frequency part of -0.01 in the Green's function. For the Brillouin-zone integration 356 \vec{q} points in the irreducible 1/48th of the zone produced well converged results. The simplest linear-mixing scheme was used to accelerate the convergence. For both cases the number of iterations ranged from 3 to 13 depending on the frequency ω .

For $\text{Ni}_{55}\text{Pd}_{45}$, we compare the results of virtual crystal (VCA), CPA, and ICPA computations, using the ICPA force constants to construct the averages used in the VCA and CPA and compare the results with experiment. We make a distinction between that use of the VCA and of "mean crystal" models in which the average mass is employed and a set of "mean-crystal" force constants are fitted as parameters to the experimental data.

Kamitakahara and Brockhouse³ investigated $\text{Ni}_{55}\text{Pd}_{45}$ by inelastic neutron scattering and reported a strange observation. A theoretical calculation based on a mean crystal model having the average mass and fitted force constants between those of Ni and Pd agreed closely with the experimental dispersion curves. This was quite a puzzle because it suggested that the large mass disorder had little effect. There were theoretical studies on this system using recursion²⁴ and the average t -matrix approximation,²⁵ but no theoretical results for the frequencies were available. In an attempt to solve this puzzle, we have carried out calculations with the CPA, the ICPA, and the VCA, as well as with the mean-crystal model used in Ref. 3.

For the ICPA calculation, we assumed that the explicit scattering caused by the force-constant disorder was confined to the nearest neighbors. This assumption is justified because the nearest-neighbor force constants are an order of magnitude larger than those of the further neighbors so that the nearest neighbors feel the effect of disorder most strongly. For the virtual crystal or the average medium into which the scattering was embedded, we kept terms in the Hamiltonian up to the fourth neighbor, which turned out to be sufficient. The problem with force constant disorder-scattering calculations is the general absence of prior information about

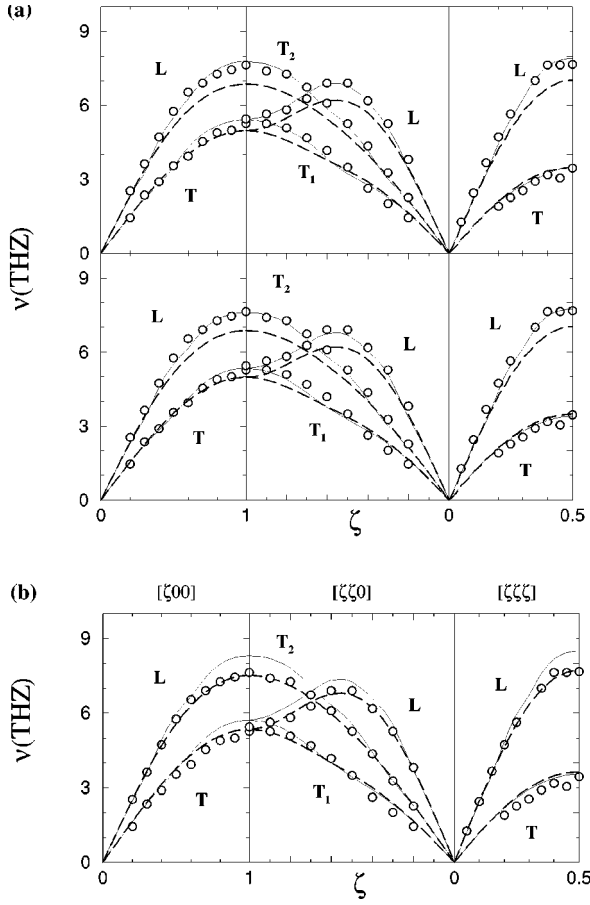


FIG. 3. (a)(Top panel) Dispersion curves (frequency ν vs reduced wave vector ζ) for $\text{Ni}_{55}\text{Pd}_{45}$ calculated in the ICPA (solid line) and in the VCA (dashed line). The circles are the experimental data (Ref. 3). (Bottom panel) Dispersion curves for $\text{Ni}_{55}\text{Pd}_{45}$ calculated in the CPA (solid line) and in the VCA (dashed line). The force constants used are given in the text. The circles are the experimental data (Ref. 3). (b) Dispersion curves for $\text{Ni}_{55}\text{Pd}_{45}$ calculated in the CPA (solid line) and in the mean-crystal model (dashed line) using the force-constants of Ref. 3. The circles are the experimental data (Ref. 3).

species-dependent force constants. We note that Pd is the larger atom here. In the alloy, the Ni-Pd separation is larger than the Ni-Ni separation. As a result, the Ni-Pd force constants should be less than the Ni-Ni ones. Using this intuitive argument and for simplicity in this illustration, we kept the $\phi_{\text{Ni-Ni}}^{\alpha\beta}$ and $\phi_{\text{Pd-Pd}}^{\alpha\beta}$ the same as those of the pure materials²² and reduced the $\phi_{\text{Ni-Pd}}^{\alpha\beta}$ below the $\phi_{\text{Ni-Ni}}^{\alpha\beta}$ by an $\alpha\beta$ -independent factor. The dispersion curves were obtained from the ICPA calculations using $\phi_{\text{Ni-Pd}}^{\alpha\beta} = 0.7\phi_{\text{Ni-Ni}}^{\alpha\beta}$ (solid lines) for the nearest neighbors and using the force constants of Ref. 3 for the higher neighbors. They are compared in the top panel of Fig. 3(a) with the experimental results³ (open circles) and the VCA for the same force constants (dashed lines). These ICPA dispersion curves were constructed by numerically determining the peaks in the coherent scattering structure factor $\langle\langle S_{\lambda}(\vec{q}, \omega) \rangle\rangle_{\text{coh}}$ given by Eq. (56), which was calculated using the partial spectral functions of Eqs. (59) and (60), and weighting them with the coherent scattering

lengths for Ni and Pd. We could thus make a direct comparison with the experimental results because the neutron data observed in the experiments inherently incorporates the effect of the scattering lengths of the species.

Excellent agreement of the ICPA with experiment was obtained for all three symmetry directions and for each branch by varying only one parameter in the force-constant matrix. This suggests that the force-constant disorder is weak and the system is dominated by the mass disorder, as one would expect from the numerical values of the parameters. It is confirmed by the results of the CPA calculations shown in the bottom panel of Fig. 3(a), using the same force constants. As in the top panel, the solid lines are the CPA results, the circles are the experimental points, and the dashed lines are the VCA results. The agreement with the experiment again suggests the dominance of the mass disorder, but there are more interesting points to note. In the long-wavelength (low \vec{q}) regime, the VCA, the CPA, and the ICPA curves are indistinguishable because the self-averaging of both mass and force constants over a single wavelength reduces both the CPA and the ICPA to the VCA. But, as we move to high wave vectors, the VCA deviates to frequencies below the experimentally observed ones. This fact is due to the use of an average mass in the Hamiltonian. In the high-wave-vector region, the lighter atoms, i.e. Ni in this case, dominate and push the frequencies up. That is why the CPA and the ICPA agree very well across the Brillouin zone while the VCA fails for the high wave vectors. The reason that Kamitakahara and Brockhouse got a very good fit to the experimental points in Ref. 3 by using their mean-crystal model is that they obtained parametrized force constants which were higher than those calculated in the VCA. Though they had used the average mass in their calculations the higher values of the force constants (They used $\bar{\Phi} = c_A\Phi_{AA} + c_B\Phi_{BB}$ rather than $\bar{\Phi} = c_{AA}^2\Phi_{AA} + c_{BB}^2\Phi_{BB} + 2c_{ACB}\Phi_{AB}$) compensated for their omission of the effect of the mass fluctuations. This is illustrated in Fig. 3(b). There, the dashed lines are their mean-crystal model calculations, the circles are the experimental points, and the solid lines represent a CPA calculation with the force constants used in Ref. 3. Here we see that the CPA yields frequencies that are too high in the large wave-vector region. The CPA captures the effect of the mass fluctuation and the domination of the Ni atoms for higher wave vectors, but the higher values of the assumed mean force constants increases the frequencies further, thereby worsening the agreement with experiment. Another striking feature is that in spite of incorporating the scattering lengths in our calculations there was little change in the ICPA results with respect to the CPA results even though the coherent scattering lengths of Ni and Pd differ significantly (the coherent scattering length for Ni is 1.03 while that of Pd is 0.6). This lack of change can be understood from a comparison between the partial and total spectral functions [Fig. 4(a)] and the partial and the total coherent structure factors [Fig. 4(b)]. In these figures, we have shown examples of ICPA spectral functions and structure factors along the $[\zeta, 0, 0]$ direction $\zeta = |\vec{q}|/|\vec{q}_{\text{max}}|$, for a low, medium, and high ζ . In each case, the peaks corresponding to the dominating species and that in the Ni-Pd curves occur at the same general positions. For

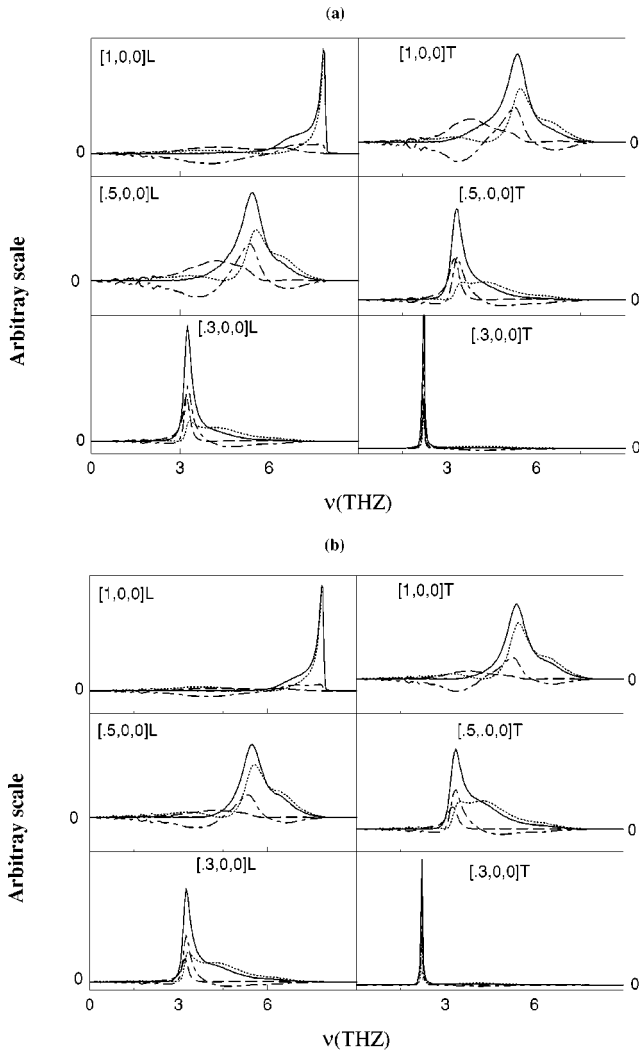


FIG. 4. (a) Partial and total spectral functions calculated in the ICPA for various ζ values in the $[\zeta, 0, 0]$ direction in $\text{Ni}_{55}\text{Pd}_{45}$. (b) Partial and total structure factors calculated in the ICPA for various ζ values in the $[\zeta, 0, 0]$ direction in $\text{Ni}_{55}\text{Pd}_{45}$. The solid lines are the total contribution, the dotted lines are the Ni-Ni spectra, the long-dashed lines are the Pd-Pd spectra, and the dot-dashed lines are the Ni-Pd contributions. The details are given in the text. The left (right) column is for longitudinal (transverse) modes.

example, in the $[0.3, 0, 0]$ -L curves, the peak in the spectral function is mostly that of Pd atoms while for the $[0.5, 0, 0]$ -L and $[1, 0, 0]$ -L curves, the contributions are from Ni atoms, the Pd-Pd contribution here is much less and that too is almost completely neutralized by the Ni-Pd contribution in the low frequency region. The coincidence of the peaks of the Ni-Pd spectral functions and those of the Ni-Ni or Pd-Pd spectral functions almost at the same position across the Brillouin zone suggests that the inclusion of scattering lengths would primarily alter the relative weights of various contributions and thereby the line shapes, while the dispersion curves would hardly change. This is demonstrated in Fig. 4(b). One can see that the weighting affects primarily the peak heights. These explicit numerical results confirm the qualitative argument given at the end of Sec. III.

The disorder-induced widths are important because they

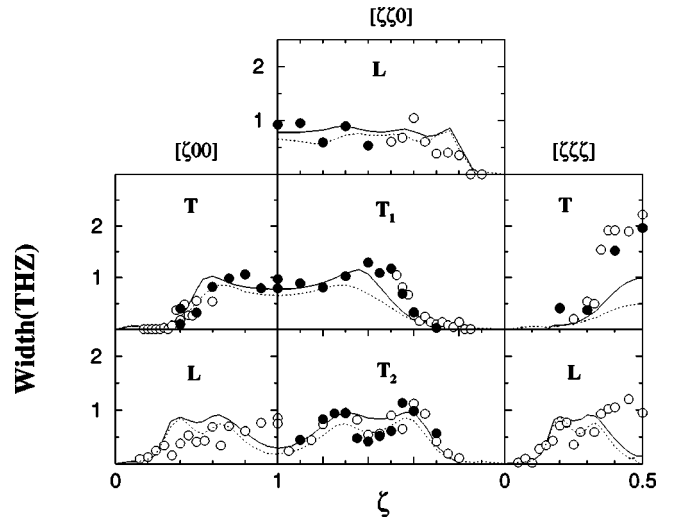


FIG. 5. Disorder-induced FWHM's in $\text{Ni}_{55}\text{Pd}_{45}$ calculated in the ICPA (solid line) and in the CPA (dotted line) using the force constants of Fig. 3(a). The circles are the widths extracted from the experimental results (Ref. 3). The filled circles had better experimental resolution.

often manifest the effect of disorder more directly than do the frequencies. Kamitakahara and Brockhouse extracted full widths at half maxima (FWHM) from their neutron groups by assuming that the observed line shape could be adequately approximated by the convolution of a Gaussian resolution function (representing the experimental resolution) with a Lorentzian natural line shape. Thus, for a comparison of our results with theirs, we have fitted our structure factors to a Lorentzian to extract the widths. The results are shown in Fig. 5. Generally, there is little difference between the widths obtained in the CPA and the ones obtained in the ICPA. In all three symmetry directions and for all branches, the ICPA performs slightly better than the CPA for high wave vectors. The worst agreement with the experiment is for high wave vectors in the $[\zeta, 0, 0]$ and $[\zeta, \zeta, \zeta]$ longitudinal branches and the $[\zeta, \zeta, \zeta]$ transverse branch. In these cases, the high values of the widths in the experimental determinations can be understood from the shape of the structure factors. From the examples in Fig. 4 one can see that the agreement with experiment is good when we have a symmetric line shape, for example, for the $[0.5, 0, 0]$ -L mode. On the other hand, the worst agreements with the experimental widths are for cases where there are highly asymmetric line shapes, for example, for the $[1, 0, 0]$ -L mode. Fitting Lorentzians to such asymmetric line shapes is not conducive to meaningful values of the FWHMs. Also, because they obtain higher widths than the theories in those particular cases which have worse resolution (open circles in Fig. 5), it is not clear that this discrepancy is significant.

The discussion above clearly tells us that for $\text{Ni}_{55}\text{Pd}_{45}$, the dominant effect is mass disorder. That alloy therefore does not provide a proper test of the ICPA. Nevertheless, our discussions have shown how a mean-crystal model can compensate for the neglect of mass fluctuations in alloys with little force constant disorder through the introduction of erroneous mean force-constants, a classic case of cancellation of errors.

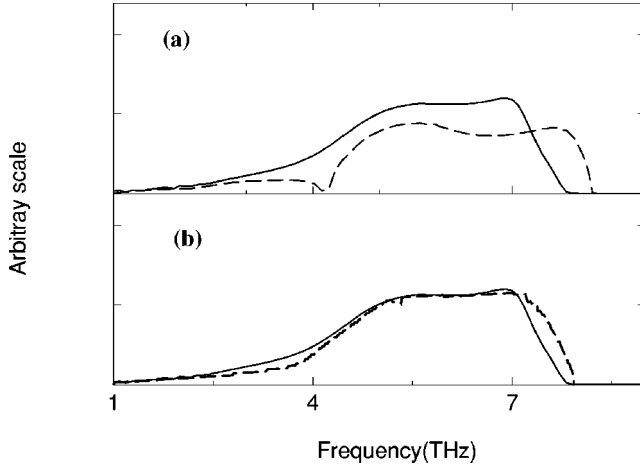


FIG. 6. (a) Incoherent neutron scattering structure factor vs frequency calculated in the ICPA (solid line) and in the CPA (dashed line) in $\text{Ni}_{50}\text{Pt}_{50}$ (b) Same plot as (a) in the ICPA (solid line) and experimental results (Ref. 4) (dashed line).

V. $\text{Ni}_{50}\text{Pt}_{50}$;

STRONG MASS AND FORCE-CONSTANT DISORDER

The mass ratio $m_{\text{Pt}}/m_{\text{Ni}}=3$, is much larger here. The force constants of Pt are, on an average, 55% larger²² than those of Ni. This makes it a potential example of strong force-constant disorder. Tsunoda *et al.*⁴ investigated $\text{Ni}_x\text{Pt}_{1-x}$ by inelastic neutron scattering and compared their observations with the CPA. Here, for illustration, we have considered $x=0.5$ only, because this is a concentrated alloy and the failure of CPA was very prominent at this concentration. They compared their incoherent scattering data with that of the CPA which predicted a split band separating out Ni and Pt contributions with a gap between them [Fig. 6(a)]. The experiments [Fig. 6(b)] did not reveal a split band, and it was very clear that the interspecies forces play a significant role. We performed calculations with the CPA and the ICPA. As before, we used the ICPA force constants in the CPA. The choice of ICPA force constants was more difficult than for the NiPd because of the larger size difference between Ni and Pt. In this alloy, the Ni-Pt separation is also larger than the Ni-Ni separation. As a result, the Ni-Pt force constants should also be less than those of Ni-Ni. Moreover, a pair of Ni atoms would find themselves in a cage partly made of larger Pt atoms which would therefore reduce the Ni-Ni force constants relative to their values in the pure material. Similarly, the bigger Pt atoms find themselves compressed between much smaller Ni atoms, which would increase the Pt-Pt force constants with respect to their values in pure Pt. Using this intuitive argument, we found that the following guesses for the force-constants worked well: $\phi_{\text{Ni-Ni}}^{xy}$, $\phi_{\text{Pt-Pt}}^{xy}$, $\phi_{\text{Ni-Ni}}^{zz}$ and $\phi_{\text{Pt-Pt}}^{zz}$ are kept the same as those of the pure materials²² and

$$\phi_{\text{Ni-Ni}}^{yy} = \phi_{\text{Ni-Ni}}^{xx} = 0.9 \phi_{\text{Ni-Ni}}^{xx}(\text{pure}),$$

$$\phi_{\text{Pt-Pt}}^{yy} = \phi_{\text{Pt-Pt}}^{xx} = 1.1 \phi_{\text{Pt-Pt}}^{xx}(\text{pure}),$$

$$\phi_{\text{Ni-Pt}}^{\alpha\beta} = 0.8 \phi_{\text{Ni-Ni}}^{\alpha\beta} \quad \text{for all } \alpha, \beta.$$

In Fig. 6, we compare the ICPA results for the incoherent

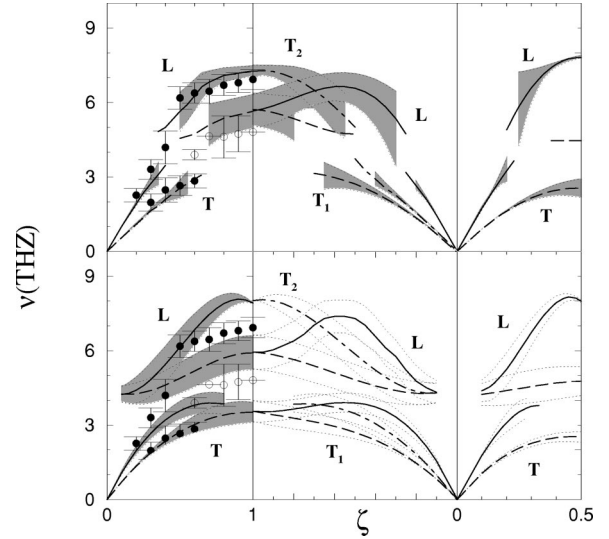


FIG. 7. The solid lines are the L branch in all the three panels, the dashed lines are the T branch in the left and the right panels. In the central column, the long-dashed curves are the T_1 branches while the dot-dashed curves are the T_2 branches. The shaded regions span the FWHM's. The circles in the left panels are the experimental data (Ref. 4). The filled ones are those with better resolution and accuracy. (Top panel) Dispersion curves for $\text{Ni}_{50}\text{Pt}_{50}$ calculated in the ICPA. (Bottom panel) Dispersion curves for $\text{Ni}_{50}\text{Pt}_{50}$ calculated in the CPA. Here, the shaded regions in the left panel span the FWHM's. In other two panels the thin dotted lines denote the FWHM's.

neutron structure factor [Eq. (54)] with those of the CPA and the experiment.⁴ The CPA shows a split-band behavior, clearly separating the low frequency Pt contribution from the high frequency Ni contribution. The overall contribution from the Pt region is much less than that of the Ni region in this system because Pt has a much lower incoherent scattering length⁴ than Ni, 0.1 in comparison to 4.5 for Ni. Including only mass fluctuations and ignoring the Ni-Pt correlated motion gives rise to this spurious gap in the CPA results as is further discussed below in connection with the coherent scattering results. On the other hand, by incorporating the force-constant disorder, as is done in the ICPA, we get rid of this spurious gap and obtain good agreement with the experimental results, including the position of the right band edge. The influence of the force-constant disorder is demonstrated more prominently in the dispersion curves and the line shapes.

In Fig. 7, we compare the dispersion curves and widths obtained in the ICPA from the coherent scattering structure factors, using the force constants as given above, with those in the CPA, using the averages of the same force-constants, and with the experimental results⁴ which are available only for the $[\zeta, 0, 0]$ directions. The ICPA agrees much better with the experiments than the CPA for both the longitudinal and the transverse branches. The CPA frequencies are generally below the experimental ones at low frequencies and above the experimental ones at high frequencies. The discrepancy gets worse as we move from the middle of the zone towards the zone edge. This is because the high wave-vector region is dominated by the lighter Ni atoms. The severity of this effect

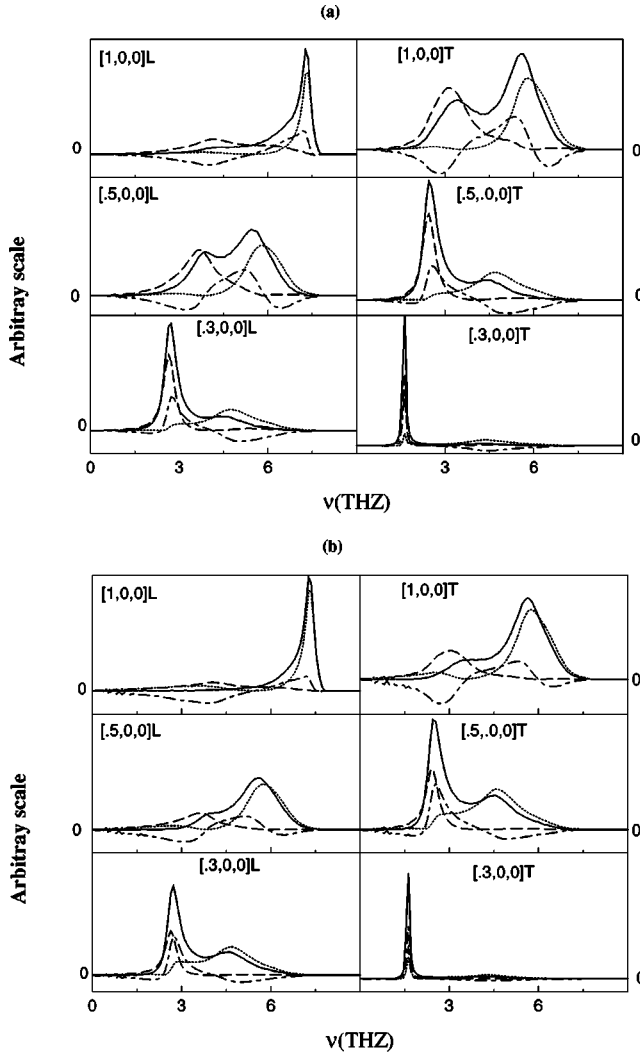


FIG. 8. (a) Partial and total spectral functions calculated in the ICPA for various ζ values in the $[\zeta,0,0]$ directions in $\text{Ni}_{50}\text{Pt}_{50}$. (b) Partial and total structure factors calculated in the ICPA for various ζ values in the $[\zeta,0,0]$ directions in $\text{Ni}_{50}\text{Pt}_{50}$. The solid lines are the total contributions, the dotted lines are the Ni-Ni contributions, the long-dashed lines are the Pt-Pt contributions, and the dot-dashed lines are the Ni-Pt contributions. The details are given in the text.

can be understood from the widths as well. In the CPA, the experimental points stay well outside the disorder-induced widths centered at the peak frequencies. The discrepancy is substantially reduced by the inclusion of force-constant disorder, as is seen from the ICPA results. Its inclusion changes the dispersion curves qualitatively as well. In the CPA, the bands extend fully across the Brillouin zone for all symmetry directions while in the ICPA, the Pt-dominated peaks disappear at high- ζ and the Ni-dominated peaks wash out at low ζ for all modes and symmetry directions, an effect observed in the experiments. This is a clear consequence of the force-constant disorder which can be understood by inspecting the spectral line shapes. In Fig. 8(a) we present the partial and the total spectral densities for three different wave-vectors. In Fig. 8(b) we present the partial and the total coherent scattering structure factors i.e., the spectral functions

weighted by the coherent scattering lengths of the species. The coherent scattering lengths of Ni and Pt differ by only 7 % (the scattering length of Ni is 1.03 while that of Pt is 0.95). However, even this small difference produces significant changes in the line shapes and in the peak frequencies. A close inspection of the various contributions reveals that unlike in NiPd, the Ni-Pt contribution plays the key role in determining the weight in the middle of the band (and in obtaining the merged bands in Fig. 6) as well as adding or subtracting weights to the Ni-Ni or Pt-Pt contributions, thus elevating or suppressing one of the peaks. For example, in Fig. 8(a), in the $[0.5,0,0]T$ curves, the Ni-Pt contribution adds weight to the total spectral function on top of the Pt-Pt peak at the low frequencies while it subtracts weight from the Ni-Ni contribution at higher frequencies thereby causing a weakly defined peak at high frequencies. In the $[0.5,0,0]L$ and in the $[1,0,0]T$ curves, the Ni-Pt contribution adds weight between the Pt-Pt and Ni-Ni peaks, thereby removing the gap in the CPA spectrum. The Ni-Pt contribution is totally due to inclusion of force-constant disorder, since diagonal disorder produces no such contribution. The effect of incorporation of the difference in scattering lengths can be seen from these two figures as well. For example, in the $[1,0,0]T$ curves, there are two well-defined peaks in the total spectral functions, whereas the low-frequency peak is transformed into a shoulder in the total structure factor. This is because Ni has the larger scattering length which enhances the weight associated with the Ni-Pt contribution thereby cancelling more effectively the contribution from the Pt-Pt part. Similar effects are seen in the $[0.5,0,0]L$ and $[1,0,0]L$ curves. Moreover, this weighting sometimes produces a weakly defined peak whose FWHM cannot be well determined, which explains the observed washing out of the dispersion curves noted above. The effect of the small difference in scattering lengths is amplified by the force-constant disorder through the Ni-Pt structure factor which plays an important role here.

In sum, the force-constant disorder plays a significant role in $\text{Ni}_{50}\text{Pt}_{50}$, and a theory with mass disorder only fails both qualitatively and quantitatively in such cases. On the other hand, the ICPA successfully explains the effects of force-constant disorder through its effect on the partial structure factors, and demonstrates the relative importance of the contributions of various atomic species to the coherent and incoherent structure factors which the CPA cannot. The ICPA and the $\text{Ni}_{50}\text{Pt}_{50}$ system therefore provide a proper test case for force-constant disorder and show that the ICPA can form a basis for understanding the lattice dynamics of other binary alloys.

VI. CONCLUSIONS

We have presented a straightforward and tractable formulation of the KLGD (Ref. 18) method for single-site scattering of phonons in three dimensional lattices. We have demonstrated how this multiple-scattering based formalism captures the effects of off-diagonal and environmental disorder. The use of augmented-space to keep track of the configurations of the system has made the formalism simple yet

powerful. The resulting translational invariance makes it numerically tractable as well. In addition, we have derived the partial Green's functions in real space as well as partial spectral functions and their sum rules. This enables one to make direct comparison with neutron scattering experiments because of the incorporation of the scattering lengths of the different species. We have applied the formalism to real random alloys. In $\text{Ni}_{55}\text{Pd}_{45}$ we have demonstrated that mass disorder plays the prominent role, and the CPA consequently does a rather good job whereas the mean-crystal model requires erroneous fitted force constants. Our partial structure factors enabled us to understand the insensitivity of the normal modes towards the difference in the coherent scattering lengths of the two species despite the significant difference of 43% in this system. The $\text{Ni}_{50}\text{Pt}_{50}$ results demonstrate the prominence of force-constant disorder even in a case where the mass ratio is 3. We have clearly demonstrated that for systems such as NiPt , where the force constants are strongly species dependent, the determination of their values is crucial. However, we had no prior information about the species dependence of the force constants. Intuitive arguments led to a set of force constants which turned out to be quite good. A better understanding of the role of disorder in the lattice dynamics of random alloys could be achieved with prior information about the force constants. These could be obtained, e.g., from first-principles calculations on a set of ordered alloys.

ACKNOWLEDGMENTS

We thank Professors David Vanderbilt, Gabriel Kotliar, and Karin Rabe for useful discussions and for the use of their computer systems. We thank W. Kamitakahara and R. Nicklow for useful communications regarding their experimental results.

APPENDIX: MATRIX ELEMENTS

For the calculations in the nearest-neighbor approximation, one needs to evaluate the $\{3(Z+1)\}^2$ matrix elements of the operators \mathbf{K}' , \mathbf{K}'^\dagger , $\tilde{\mathbf{V}}(\vec{q})$, and \mathbf{G}_{vca}^{-1} and use them as inputs. These evaluations are done in augmented space using Eq. (14). The symmetry of the lattice structure is used to reduce the number of matrix elements evaluated. Here, we give results only for an fcc lattice. All the matrices are, therefore, of dimension 39×39 .

In an fcc system, each atom has 12 nearest neighbors with coordinates $(\pm \frac{1}{2}, \pm \frac{1}{2}, 0)$, $(\pm \frac{1}{2}, 0, \pm \frac{1}{2})$, and $(0, \pm \frac{1}{2}, \pm \frac{1}{2})$ with respect to the coordinates of the reference atom at $(0,0,0)$. The force constants, between the atom 0 and its neighbors satisfy the following cubic symmetry relation:

$$\phi_{0j}^{\alpha\beta} = \phi_{0j}^{\beta\alpha} = \phi_{j0}^{\alpha\beta} = \phi_{0k}^{\alpha\beta}, \quad (\text{A1})$$

where $\vec{R}_{0j} = -\vec{R}_{0k}$ and k and j are two neighbors on opposite sides of site 0. For example, the force-constant matrix between the atoms $(0,0,0)$ and $(\frac{1}{2}, \frac{1}{2}, 0)$ is of the form

$$\phi_{(000, \frac{1}{2} \frac{1}{2} 0)} = \begin{pmatrix} a & b & 0 \\ b & a & 0 \\ 0 & 0 & g \end{pmatrix}. \quad (\text{A2})$$

The force-constant matrices between the atom 0 and its other neighbors can easily be calculated from Eq. (A2) via the cubic symmetry operations. The results are

$$\begin{aligned} (G_{vca}^{-1})_{ij}^{\alpha\beta} &= \bar{m}\omega^2 - 8D_1^{xx} - 4D_1'^{xx} \quad \text{if } i=j, \alpha=\beta, \\ &= 0 \quad \text{if } i=j, \alpha \neq \beta, \\ &= D_1'^{xx} \quad \text{if } i=0, j=n=1-12, \alpha=\beta, R_j^\alpha=0, \\ &= D_1^{xx} \quad \text{if } i=0, j=n=1-12, \alpha=\beta, R_j^\alpha \neq 0, \\ &= 2R_j^\alpha \times 2R_j^\beta \times D_1^{xy} \quad \text{if } i=0, j=n=1-12, \alpha \neq \beta, \\ &= 0 \quad \text{otherwise} \end{aligned} \quad (\text{A3})$$

and

$$(G_{vca}^{-1})_{ij}^{\alpha\beta} = (G_{vca}^{-1})_{ji}^{\alpha\beta} = (G_{vca}^{-1})_{ij}^{\beta\alpha} \quad \text{for all } i, j, \alpha, \text{ and } \beta.$$

Also, we find

$$\begin{aligned} (K')_{ij}^{\alpha\beta} &= m'\omega^2 - 8D_2^{xx} - 4D_2'^{xx} \quad \text{if } i=j=0, \alpha=\beta, \\ &= 0 \quad \text{if } i=j=0, \alpha \neq \beta, \\ &= D_2'^{xx} \quad \text{if } i=0, j=n=1-12, \alpha=\beta, R_j^\alpha=0, \\ &= D_2^{xx} \quad \text{if } i=0, j=n=1-12, \alpha=\beta, R_j^\alpha \neq 0, \\ &= 2R_j^\alpha \times 2R_j^\beta \times D_2^{xy} \quad \text{if } i=0, j=n=1-12, \alpha \neq \beta, \\ &= -(K')_{0j}^{\alpha\beta} \quad \text{if } i \neq 0, j=i=n=1-12, \\ &= 0 \quad \text{otherwise} \end{aligned} \quad (\text{A4})$$

and

$$(K')_{ij}^{\alpha\beta} = (K')_{ji}^{\alpha\beta} = (K')_{ij}^{\beta\alpha} \quad \text{for all } i, j, \alpha, \text{ and } \beta.$$

Similarly, we obtain

$$\begin{aligned} \tilde{\mathbf{V}}(\vec{q})_{ij}^{\alpha\beta} &= L^\alpha \quad \text{if } i=j=0, \alpha=\beta, \\ &= 4D_3^{xy} \sin(q_\alpha) \sin(q_\beta) \quad \text{if } i=j=0, \alpha \neq \beta, \\ &= D_5 \quad \text{if } i=0, j=n=1-12, \alpha=\beta, R_j^\alpha=0, \\ &= D_6 \quad \text{if } i=0, j=n=1-12, \alpha=\beta, R_j^\alpha \neq 0, \\ &= 2R_j^\alpha \times 2R_j^\beta \times D_7 \quad \text{if } i=0, j=n=1-12, \alpha \neq \beta, \end{aligned}$$

$$\begin{aligned}
 &= D_4'^{xx} - D_1'^{xx} \quad \text{if } i \neq 0, j = i = n = 1 - 12, \\
 &\quad \alpha = \beta, R_i^\alpha = 0, \\
 &= D_4^{xx} - D_1^{xx} \quad \text{if } i \neq 0, j = i = n = 1 - 12, \\
 &\quad \alpha \beta, R_i^\alpha \neq 0, \\
 &= 2R_j^\alpha \times 2R_j^\beta \times (D_4^{xy} - D_1^{xy}) \quad \text{if } i \neq 0, \\
 &\quad j = i = n = 1 - 12, \alpha \neq \beta, \\
 &= -D_3'^{xx} e^{i\vec{q} \cdot \vec{R}_i} \quad \text{if } j \neq i = n = 1 - 12, \vec{R}_j = -\vec{R}_i, \\
 &\quad \alpha = \beta, R_j^\alpha = 0, \\
 &= -D_3^{xx} e^{i\vec{q} \cdot \vec{R}_i} \quad \text{if } j \neq i = n = 1 - 12, \vec{R}_j = -\vec{R}_i, \\
 &\quad \alpha = \beta, R_j^\alpha \neq 0, \\
 &= -D_3^{xy} e^{i\vec{q} \cdot \vec{R}_i} \times 2R_i^\alpha \times 2R_i^\beta \quad \text{if } j \neq i = n = 1 - 12, \vec{R}_j \\
 &= -\vec{R}_i, \alpha \neq \beta, \\
 &= 0 \quad \text{otherwise,} \tag{A5}
 \end{aligned}$$

and

$$\tilde{V}(\vec{q})_{ij}^{\alpha\beta} = (\tilde{V}(\vec{q})^*)_{ji}^{\alpha\beta} = \tilde{V}(\vec{q})_{ij}^{\beta\alpha}, \quad \text{for all } i, j, \alpha, \text{ and } \beta.$$

In these evaluations, we have used the notation $R_{0j} = R_j$, $n = 1 - 12$ to represent the 12 nearest neighbors, and the notations

$$\begin{aligned}
 \bar{m} &= c_A m^A + c_B m^B, \\
 m' &= \sqrt{c_A c_B} (m^A - m^B), \\
 \tilde{m} &= c_B m^A + c_A m^B, \\
 D_1^{xx} &= c_A^2 a_{AA} + c_B^2 a_{BB} + 2c_A c_B a_{AB}, \\
 D_1'^{xx} &= c_A^2 g_{AA} + c_B^2 g_{BB} + 2c_A c_B g_{AB}, \\
 D_1^{xy} &= c_A^2 b_{AA} + c_B^2 b_{BB} + 2c_A c_B b_{AB}, \\
 D_2^{xx} &= \sqrt{c_A c_B} \{c_A a_{AA} - c_B a_{BB} + (c_B - c_A) a_{AB}\}, \\
 D_2'^{xx} &= \sqrt{c_A c_B} \{c_A g_{AA} - c_B g_{BB} + (c_B - c_A) g_{AB}\}, \\
 D_2^{xy} &= \sqrt{c_A c_B} \{c_A b_{AA} - c_B b_{BB} + (c_B - c_A) b_{AB}\}, \\
 D_3^{xx} &= c_A c_B (a_{AA} + a_{BB} - 2a_{AB}), \\
 D_3'^{xx} &= c_A c_B (g_{AA} + g_{BB} - 2g_{AB}), \\
 D_3^{xy} &= c_A c_B (b_{AA} + b_{BB} - 2b_{AB}), \\
 D_4^{xx} &= c_A c_B (a_{AA} + a_{BB}) + (c_A^2 + c_B^2) a_{AB},
 \end{aligned}$$

$$\begin{aligned}
 D_4'^{xx} &= c_A c_B (g_{AA} + g_{BB}) + (c_A^2 + c_B^2) g_{AB}, \\
 D_4^{xy} &= c_A c_B (b_{AA} + b_{BB}) + (c_A^2 + c_B^2) b_{AB}, \\
 D_5 &= (D_1^{xx} - D_4^{xx}) + D_3^{xx} e^{i\vec{q} \cdot \vec{R}_j}, \\
 D_6 &= (D_1^{xy} - D_4^{xy}) + D_3^{xy} e^{i\vec{q} \cdot \vec{R}_j}, \\
 D_7 &= (D_1'^{xx} - D_4'^{xx}) + D_3'^{xx} e^{i\vec{q} \cdot \vec{R}_j}, \\
 L^\alpha &= (\bar{m} - \tilde{m}) \omega^2 - 8(D_1^{xx} - D_4^{xx}) - 4(D_1'^{xx} - D_4'^{xx}) \\
 &\quad - 4D_3^{xx} \{\cos q_\alpha (\cos q_\gamma + \cos q_\delta) \\
 &\quad - 4D_3'^{xx} \cos q_\gamma \cos q_\delta; \quad \gamma, \delta \neq \alpha. \tag{A6}
 \end{aligned}$$

The symmetries of the force-constant matrices are reflected in the operators as well. The effect of itineration is captured in $\tilde{V}(\vec{q})_{ij}^{\alpha\beta}$ through the quantities $D_3^{\alpha\beta}$. When there is no force-constant disorder the D_3 terms vanish and \tilde{V} becomes independent of \vec{q} . A \vec{q} -independent self-energy results, and we arrive at the CPA equations. As an example of how to obtain the various matrix elements of the operators, we present the calculation of $K_{01}'^{(0)}$ where $R_1 = (\frac{1}{2}, \frac{1}{2}, 0)$:

$$\begin{aligned}
 K_{01}'^{(0)} &= \langle 0f | \hat{\mathbf{K}} | 1f_0 \rangle, \\
 &= \langle 0f | (\hat{\mathbf{m}} \cdot \omega^2 - \hat{\Phi}) | 1f_0 \rangle.
 \end{aligned}$$

Using Eqs. (6) and (11),

$$\langle 0f | \hat{\mathbf{m}} | 1f_0 \rangle = 0,$$

and using Eqs. (7) and (11),

$$\begin{aligned}
 \langle 0f | \hat{\Phi} | 1f_0 \rangle &= \langle f | \hat{\Phi}_{01} | f_0 \rangle, \\
 &= \langle (\sqrt{c_A} \langle A_0 | + \sqrt{c_B} \langle B_0 |), (\sqrt{c_A} \langle A_1 | \\
 &\quad + \sqrt{c_B} \langle B_1 |) | \{ \phi_{01}^{AA} \hat{\eta}_0^A \hat{\eta}_1^A + \phi_{01}^{BB} \hat{\eta}_0^B \hat{\eta}_1^B \\
 &\quad + \phi_{01}^{AB} \hat{\eta}_0^A \hat{\eta}_1^B + \phi_{01}^{BA} \hat{\eta}_0^B \hat{\eta}_1^A \} | (\sqrt{c_B} | A_0 \rangle \\
 &\quad - \sqrt{c_A} | B_0 \rangle), (\sqrt{c_A} | A_1 \rangle + \sqrt{c_B} | B_1 \rangle) \rangle.
 \end{aligned}$$

If we use the Cartesian coordinates explicitly, then the xx component is, for example,

$$\langle f | \Phi_{01}^{xx} | f_0 \rangle = \sqrt{c_A c_B} \{c_A a_{AA} - c_B a_{BB} + (c_B - c_A) a_{AB}\} = D_2^{xx}.$$

- ¹B. Mozer, K. Otnes, and V. W. Myers, Phys. Rev. Lett. **8**, 278 (1962); B. Mozer, K. Otnes, and C. Thaper, Phys. Rev. **152**, 535 (1966); E. C. Svensson, B. N. Brockhouse, and J.M. Rowe, Solid State Commun. **3**, 245 (1965); E. C. Svensson and B. N. Brockhouse, Phys. Rev. Lett. **18**, 858 (1967); H. G. Smith, and M. K. Wilkinson, *ibid.* **20**, 1245 (1968); R. M. Nicklow, P. R. Vijayraghavan, H. G. Smith and M. K. Wilkinson, in *Neutron Inelastic Scattering* (IAEA, Vienns, 1968), Vol. I, p. 47.
- ²R. M. Cunnigham, L. D. Muhlestein, W. M. Shaw, and C. W. Tompson, Phys. Rev. B **2**, 4864 (1970); N. Wakabayashi, R.M. Nicklow, and H. G. Smith, *ibid.* **4**, 2558 (1971); E. C. Svensson and W. A. Kamitakahara, Can. J. Phys. **49**, 2291 (1971); N. Wakabayashi, Phys. Rev. B **8**, 6015 (1973); B. N. Brockhouse and R. M. Nicklow, Bull. Am. Phys. Soc. **18**, 112 (1973); A. Zinken, U. Buchenau, H. J. Fenzel, and H. R. Schober, Solid State Commun. **13**, 495 (1977).
- ³W. A. Kamitakahara and B. N. Brockhouse, Phys. Rev. B **10**, 1200 (1974).
- ⁴Y. Tsunoda, N. Kunitomi, N. Wakabayashi, R.M. Nicklow, and H. G. Smith, Phys. Rev. B **19**, 2876 (1979).
- ⁵R. M. Nicklow in *Methods of Experimental Physics* (Academic Press, New York, 1983), Vol. 23, p. 172.
- ⁶D. W. Taylor, Phys. Rev. **156**, 1017 (1967).
- ⁷N. Kunimoto, Y. Tsunoda, and Y. Hirai, Solid State Commun. **13**, 495 (1973); T. Kaplan and M. Mostoller, Phys. Rev. B **9**, 353 (1974); W. A. Kamitakahara, Bull. Am. Phys. Soc. **19**, 321 (1974).
- ⁸W. A. Kamitakahara and D. W. Taylor, Phys. Rev. B **10**, 1190 (1974); M. Mostoller, T. Kaplan, N. Wakabayashi, and R. M. Nicklow, *ibid.* **10**, 3144 (1974); H. G. Smith and N. Wakabayashi, Bull. Am. Phys. Soc. **21**, 410 (1976).
- ⁹H. Shiba, Prog. Theor. Phys. **40**, 942 (1968).
- ¹⁰T. Kaplan and M. Mostoller, Phys. Rev. B **9**, 1783 (1974).
- ¹¹S. Takeno, Prog. Theor. Phys. **40**, 942 (1968).
- ¹²B. G. Nickel and W. H. Butler, Phys. Rev. Lett. **30**, 363 (1973).
- ¹³F. Ducastelle, J. Phys. C **7**, 1795 (1974); J. Mertsching, Phys. Status Solidi B **63**, 241 (1974).
- ¹⁴A. Gonis and J. W. Garland, Phys. Rev. B **18**, 3999 (1978).
- ¹⁵R. Haydock, V. Heine, and M. J. Kelly, J. Phys. C **5**, 2845 (1975).
- ¹⁶M. Yussouff and A. Mookerjee, J. Phys. C **17**, 1009 (1984).
- ¹⁷A. Mookerjee, J. Phys. C **6**, L205 (1973).
- ¹⁸T. Kaplan, P. L. Leath, L. J. Gray, and H. W. Diehl, Phys. Rev. B **21**, 4230 (1980).
- ¹⁹R. Mills and P. Ratanavararaksha, Phys. Rev. B **18**, 5291 (1978).
- ²⁰R. J. Elliott, J. A. Krumhansl, and P. L. Leath, Rev. Mod. Phys. **46**, 465 (1974).
- ²¹T. Kaplan and L. J. Gray, Phys. Rev. B **14**, 3462 (1976).
- ²²D. H. Dutton, B. N. Brockhouse, and A. P. Miller, Can. J. Phys. **50**, 2915 (1972).
- ²³E. C. Svensson, B. N. Brockhouse, and J. M. Rowe, Phys. Rev. **155**, 619 (1967).
- ²⁴A. Mookerjee and R. P. Singh, J. Phys. F: Met. Phys. **18**, 2171 (1988).
- ²⁵W. A. Kamitakahara and D. W. Taylor, Phys. Rev. B **10**, 1190 (1974).
- ²⁶A. C. Aitken, in *Determinants and Matrices* (Interscience, New York, 1956).
- ²⁷S. M. Chitanvis and P. L. Leath, J. Phys. C **16**, 1049 (1983).
- ²⁸A. Gonis, in *Green Functions for Ordered and Disordered Systems* (North-Holland, Amsterdam, 1992), p. 141.